ELECTROSTATIC BURSTS GENERATED BY ELECTRONS TRAPPED IN WHISTLER MODE CHORUS WAVE FIELDS

by

Lee Allen Reinleitner

A thesis submitted in partial fulfillment
of the requirements for the degree of
Doctor of Philosophy in Physics
in the Graduate College of
The University of Iowa

July, 1982

Thesis supervisor: Professor Donald A. Gurnett

Graduate College
The University of Iowa
Iowa City, Iowa

CERTIFICATE OF APPROVAL

PH.D. THESIS

This is to certify that the Ph.D thesis of

Lee Allen Reinleitner

has been approved by the Examining Committee for the thesis requirement for the Doctor of Philosophy degree in Physics at the July, 1982 graduation.

Thesis committee: Daniel A. Hunt
Thesis supervisor

J. A. Van Allen
Member

Stanley Shawhan
Member

Robert P. Merlino
Member

John Robinson
Member

ACKNOWLEDGEMENTS

My sincerest thanks go to my advisor, Dr. Donald Gurnett, who guided my earlier studies and interests in space physics. His invaluable advice and guidance throughout my graduate career, and especially during the work covered in this manuscript, are greatly appreciated. I wish also to thank Dennis Gallagher for his patience and expert help when using the Univac 418 computer, as well as discussions of great aid to the work included in this thesis. His friendship and help are part of what has made my graduate career at the University of Iowa so very special. I wish to thank Dr. Roger R. Anderson for his aid in acquisition and interpretation of the ISEE 1 and ISEE 2 data, as well as other satellite data made available.

I wish to thank Dr. Louis Frank for permission to use the LEPEDEA data on the ISEE 1 spacecraft, and to especially thank Dr. Timothy Eastman for his great assistance in reducing, understanding, and interpreting the LEPEDEA data.

For their role in data reduction and outputs, I wish to thank Mark Brown, Paul Holland, Dora Walker, Terrance Averkamp, and Dick West. I also greatly appreciate the skillful work put into drafting figures done by Joyce Chrisinger, John Birkbeck, and Jeana Wonderlich. I wish to especially thank Kathy Goodner who typed part of this manuscript, helped edit other parts, and aided in use of the word processor.

This research was supported by NASA through grants NGL-16-001-002 and NGL-16-001-043 from NASA Headquarters and contracts NAS5-20093, NAS5-26819, AND NAS5-11074 with Goddard Space Flight Center, and the Office of Naval Research. The LEPEDEA data reduction from the ISEE 1 instrument was performed through contract NAS5-26257 with Goddard Space Flight Center. I would like to gratefully acknowledge the Graduate College of the University of Iowa, for the Teaching-Research Fellowship support during the first four years of my graduate career.

ABSTRACT

Recent studies of wideband plasma wave data from the ISEE-1 and ISEE-2 spacecraft have revealed that whistler mode chorus emissions in the Earth's outer magnetosphere are often accompanied by high frequency bursts of electrostatic waves with a frequency below the electron plasma frequency. Investigations have shown that in some cases the electrostatic waves are found to be modulated at the chorus frequency. Further studies indicate through use of LEPEDEA data on ISEE-1 that these bursts are being produced by a "beam" of electrons trapped in Landau (longitudinal) resonance in effective potential wells of the chorus wave and thus moving at the chorus phase velocity. There seems to be a lower threshold in chorus intensity, below which the electrostatic bursts do not appear.

The high frequency electrostatic waves appear to be caused by a type of two-stream instability called the resistive-medium instability, produced by these trapped electrons. The reduction in the electrostatic burst frequency to below the plasma frequency is a characteristic of the resistive-medium instability. The instability is applicable only in the regime where V_o/V_T is on the order of 1, where V_o is the velocity of the beam and V_T is the averaged thermal velocity of the plasma electrons. The derivation assumes cold ions but warm electrons in the plasma. The instability requires Landau damping to operate, and thus the beam

velocity must be in the steep slope region of the plasma electron distribution function rather than the high velocity tail region. In examined cases from LEPEDEA data the electron thermal energies are on the order of a few hundred eV. The beam velocities in the observed cases were ≈400 eV and ≈630 eV, thus verifying that the electrostatic bursts are in the proper regime for the resistive-medium instability. Evidence is given that the resistive-medium instability is a plausible generation mechanism for the electrostatic bursts.

Several cases are examined which suggest the relevance of these electrostatic bursts to features observed in space physics data for regions other than the Earth's magnetosphere.

TABLE OF CONTENTS

LIST OF FIGURES

I. INTRODUCTION

The Earth's magnetosphere has proven to be a rich source of various types of plasma wave modes. This study treats a type of electrostatic wave that appears in very sharply defined bursts, and is closely correlated with a type of electromagnetic whistler mode wave known as chorus. These waves occur in the outer magnetosphere, just inside of the magnetopause boundary layer, on the dayside region of the magnetosphere.

Chorus waves are a type of low frequency electromagnetic wave phenomenon in the magnetosphere that are believed to result from a gyroresonance interaction with energetic electrons. The frequency range of chorus emissions in the outer magnetosphere is approximately 100 Hz to 800 Hz. Chorus usually has a well-defined frequency, and often has discrete frequency-time features, consisting of narrowband tones increasing in frequency with increasing time [Helliwell, 1965]. Chorus also occurs as a simple banded emission with little or no structure [Burtis and Helliwell, 1969].

On the dayside of the Earth, chorus waves are generated by electrons with energies in the range of 5 - 150 keV [Burton and Holzer, 1974], and on the nightside of the Earth are associated with magnetic substorm electrons of energies > 40 keV [Tsurutani and Smith, 1974]. The generation mechanism is believed to be a Doppler-shifted cyclotron resonance with these high energy electrons [Dowden, 1962; Brice, 1964;

and Helliwell, 1967]. The generation region is always near the equatorial regions [Helliwell, 1967; Helliwell and Inan, 1982]. The Doppler-shifted electron cyclotron resonance condition is given by Equation 1

$$k_{\parallel} v_{\parallel} = \omega - m|\Omega^{-}| \qquad \text{where } m = 0, 1, 2, \ldots \text{ are integers,} \qquad (1)$$

$v_{\parallel}$ and $k_{\parallel}$ are velocity and wave vector parallel to the magnetic field, ω is the angular wave frequency, and Ω^{-} is the electron gyrofrequency.

For cyclotron resonance, the integer m must not be equal to zero. The special case where m is zero is called the Landau resonance. A careful analysis reveals that the whistler mode is unstable if a positive pitch angle anisotropy exists in the electron distribution function at the resonance velocity [Kennel and Petschek, 1966]. A positive pitch angle anisotropy occurs whenever a loss cone exists in the electron angular distribution. The electrons resonanting with the wave will be pitch angle scattered to a smaller pitch angle value, thus precipitating electrons along the magnetic field line direction. It is important to note from Equation 1 that the resonanting electrons are moving in a direction along the field line opposite to the direction of the chorus whistler mode wave. Precipitating electrons have been reported [Oliven and Gurnett, 1968; Rosenberg et al., 1971] which are associated with chorus emissions and are believed to be pitch angle scattered by these waves. Since the growth mechanism requires a wave to start the process, the discrete emissions are believed to be triggered by either natural waves of small amplitude such as hiss [Koons, 1981] artificial wave

injections [Helliwell and Katsufrakis, 1974], or possibly signals from electric power transmission lines [Luette et al., 1977]. Once generated, the discrete frequency of the emission will raise and fall in various patterns depending on the motion of the generating electrons toward or away from the equatorial region.

Chorus has been known for many years [Helliwell, 1965] to be propagating in the whistler mode. The index of refraction of the whistler mode is given to a good approximation by Equation 2, from Stix [1962],

$$n^2 = 1 - \frac{\omega_{pe}^2}{\omega(\omega - \omega_{ge}\cos\theta)} \qquad (2)$$

where n is the index of refraction, ω_{pe} is the electron plasma frequency, ω is the wave frequency, ω_{ge} is the electron gyrofrequency, and θ is the angle between the wave vector $\vec{k}$ and the ambient magnetic field. Chorus thus propagates in a dispersive manner with a velocity much lower than the speed of light in a vacuum. For the parameters found in this study, the chorus phase velocity was on the order of 1/10 to 1/20 of the speed of light in a vacuum. Although the ray path of the chorus wave tends to follow the ambient field line, the wave vector can be at a substantial angle θ to the field line [Kennel and Thorne, 1967; Burton and Holzer, 1974; Burtis and Helliwell, 1976]. The general magnitude of θ is still a subject of some debate due to the lack of wave normal measurements but is generally believed to be in the range from about 0 to 30° [B. T. Tsurutani, private communication, 1982].

The electrostatic bursts analyzed in this study have a frequency much greater than that of the chorus. The frequency is usually somewhat lower than the electron plasma frequency, and is normally in the range from about 3 kHz up to 10 kHz. The electrostatic bursts appear to be a longitudinal electrostatic wave with a wave vector aligned almost directly along the ambient magnetic field. In some cases, the amplitude of the electrostatic bursts is shown to have a modulation at the chorus frequency. This modulation suggests a strong physical interaction between these two wave modes.

This study details the investigation of this interaction and provides very strong evidence that the electrons responsible for the electrostatic bursts are trapped and accelerated by a Landau resonance interaction with the chorus wave. Particles in Landau resonance with a wave have a parallel velocity that matches the wave phase velocity along the field line. This condition is also contained in the generalized resonance condition given by Equation 1, by setting m equal to zero. Equation 1 with $m = 0$ is satisfied when the resonant electrons have a velocity $v_{\parallel}$ along the ambient field line equal to the phase velocity component of the whistler mode chorus wave along the field line ($\omega/k_{\parallel}$). If the wave amplitude is sufficiently large, the Landau resonance can lead to trapping of the particles in the potential well produced by the wave. Evidence for this resonant trapping includes detection of an electron enhancement that is aligned along the ambient magnetic field, by use of the LEPEDEA detector on the ISEE 1 spacecraft. This enhancement is referred to as a beam in this study, though careful examination shows that it may not correspond to an idealized delta function beam.

This study shows the first clear evidence that Landau resonant trapping occurs because of whistler mode chorus waves. Recently the theory of Landau (longitudinal) resonance with whistler mode waves has been studied by Inan and Tkalcevic [1982].

Evidence is presented that the electron "beam", which has a velocity on the same order as the electron thermal velocity of the plasma, produces the electrostatic bursts by a specific type of two-stream instability called a resistive-medium instability. This resistive-medium instability is distinguishable from the usual bump-on-tail instability primarily by a frequency downshift below the electron plasma frequency. Significant evidence is presented that this resistive-medium instability is the operational instability for the electrostatic bursts described in this study.

This study describes both the observations and the theoretical model used to show the cohesiveness of these observations. The organization of the material is as follows: Section II deals with the instrumentation on the ISEE 1 and ISEE 2 spacecraft, which were used for most of the data in the study. Section III contains the main observational characteristics of the electrostatic bursts, and the relationship to the whistler mode chorus waves. The observed relationship suggests a simple model for the interaction between the the chorus wave and the electrostatic bursts, that is mediated by electrons trapped in Landau or longitudinal resonance with the chorus wave. This simple model is outlined in Section IV. To confirm the model, LEPEDEA particle data was investigated to try to observe the trapped electrons, and Section V contains

the results of this successful search. Section VI covers the resistive-medium instability theory, and evidence that it correctly explains the observational characteristics of the electrostatic bursts. Section VII outlines some possibly related phenomenon, and the summary and conclusion are contained in Section VIII. Appendix A contains the derivation of the resistive-medium instability. Appendix B explains the particle trapping computer simulation used in this study, while Appendix C contains the Figures for this manuscript.

II. DESCRIPTION OF SATELLITE INSTRUMENTATION

A. Spacecraft and Orbital Characteristics

The primary data used in this work was obtained from the ISEE 1 and ISEE 2 (International Sun-Earth Explorer) spacecraft, which were launched into Earth orbit simultaneously on October 22, 1977. These two spacecraft are in almost identical orbits, with a separation of only a few hundred kilometers in the region where most of the data for this work were taken. The orbit is very eccentric, with an apogee geocentric radial distance of 22.5 R_E, and a perigee of 1.12 R_E. A typical orbit illustrated in Figure 1. The orbit is generally equatorial with an inclination of about 30 degrees to the ecliptic plane [Anderson et al., 1981]. The purpose of the two spacecraft was to obtain simultaneous measurements in order to separate spatial and temporal effects. The orbital period is 57.3 hours for both spacecraft.

The ISEE 1 spacecraft has a spin period of three seconds. The spacecraft rotation is valuable in determining many plasma wave parameters. This rotation is also used to obtain a complete scan over all angles for the LEPEDEA data.

The local time of the apogee at launch was about 10 hours, and it decreases at a rate of about 2 hours per month. This means that as seen from the solar ecliptic geocentric coordinates, the ISEE orbit precesses an entire 360 degrees in one year. This precession carries the

spacecraft into very different regions of the magnetosphere at different times of the year.

B. Plasma Wave Data on the ISEE Spacecraft

The predominant source of the data utilized for this study was the ISEE 1 spacecraft which is shown in Figure 2. All of the plasma wave data used was obtained from the University of Iowa Plasma Wave Experiment on the ISEE 1 and ISEE 2 spacecraft. The instrumentation used for the plasma wave data is described in detail in Gurnett et al. [1978].

The most commonly used part of the Plasma Wave Experiment was the wideband receiver with selectable 10- and 40-kHz bandwidths and any of eight selectable base frequencies from 0 Hz to 2 MHz. The wideband mode used for this work used two frequency channels, one from 650 Hz to 10 kHz which directly modulates the wideband transmitter, and the other from 10 Hz to 1 kHz which is transmitted using an FM subcarrier. The ISEE 2 wideband receiver is identical to the ISEE 1 receiver except that it is limited to only a 10-kHz bandwidth. The wideband receivers were used to provide analog waveforms of the received signals. Due to the large dynamic range the wideband receiver was provided with an Automatic Gain Control (AGC) which maintained a nearly constant signal amplitude. Sometimes real signal strength variations are masked by the AGC. An example is the lack of spin modulation on the electrostatic bursts which is described in Section III.

High time resolution spectrum measurements were also available on ISEE 1 from a 20-channel electric spectrum analyzer which covered a

range from 5.62 Hz to 311 kHz, and a 14-channel magnetic spectrum analyzer covering the frequency range from 5.62 Hz to 10 kHz. Although a choice of several different antennas for the electric field measurements was possible, in these observations the antenna used was the fine wire long electric dipole antenna (v axis) which had a 215 meter tip-to-tip length, and was shared with the Heppner dc electric-field experiment. The magnetic spectrum analyzer was connected to a magnetic search coil antenna. These analyzers have four frequency channels per decade and bandwidths of ±15% up to 10 kHz and ±7.5% above 10 kHz. For ISEE 2 a single 16-channel spectrum analyzer was provided with a frequency range from 5.6 Hz to 31.1 kHz. This spectrum analyzer was selectable for either electric field measurements from a 30 meter electric dipole antenna, or magnetic field fluctuation measurements from the magnetic search coil antenna. The sample rate is 1 sample/s in low bit rate, and 4 samples/s in high bit rate. In addition, a rapid sample mode for the electric spectrum analyzer was available. In this mode 32 samples/s could be made on any one frequency channel. The channels being thus sampled were continuously rotated.

C. LEPEDEA Instrumentation

Extremely valuable data on the electrons and ions were obtained from the University of Iowa Quadrispherical LEPEDEA (Low Energy Proton and Electron Differential Energy Analyzer) data. Full descriptions of the LEPEDEA instrument are given by Frank et al. [1978 a,b]. The LEPEDEA instrument samples ion and electron velocity distributions over approximately 98 percent of the unit sphere. This coverage is obtained

by the use of seven pairs of sensors which are used to segment the overall field of view of 6 x 162 degrees into seven contiguous fields-of-view along the major axis. This coverage is illustrated in Figure 3, where we can observe that as the spacecraft spins, the field-of-view of the seven detector pairs covers all except ~ 2% of the entire unit sphere. Twelve azimuthal sectors are used for the high bit rate mode, so that the angle ϕ shown in Figure 3 is divided into 12 contiguous and equal segments. Thus the entire unit sphere is divided into 12 x 7 = 84 segments.

The instruments have an energy resolution of $\Delta E/E = 0.16$, and cover an energy range of 1 eV to 45 keV for positive ions and electrons in the all energy mode. In the high bit rate mode used for all cases in this investigation, an instrument cycle requires 128 seconds to obtain a full velocity distribution function (32 energy levels x 4 seconds per energy level). With 12 azimuthal sectors, 7 polar angles, and 32 sampled energy levels, a total of 2688 samples of velocity space are obtained in the 128 second period of high bit rate data.

The primary LEPEDEA data output used in this work was the E-ϕ spectrogram plot form. An example of one E-ϕ plot format is shown in Figure 4. The standard format uses fifteen of these plots for the entire data display. There are seven plots for the seven ion detectors (marked with the detector number and P for proton), and seven plots for the electron detectors (marked with the detector number and E for electron). An additional central panel marked GM for Geiger-Mueller tube, which has a 40 degree field of view, provides measurements of the angular distributions of $\gtrsim$ 45 keV electrons in the spin plane of the spacecraft.

Starting at the lowest energy, the fourteen electron and proton detectors are sampled simultaneously at ≈ 0.25 second intervals at one energy level for 4.0 seconds (one spin period = 3.0 seconds). Thus the entire azimuthal angle ϕ is covered at one energy before moving up to the next energy level. This means that the ordinate represents both increasing energy and increasing time as shown in Figure 4 [Eastman and Frank, 1982]. The instrument cycle time is 128 seconds in the high bit rate mode. The time displayed on each E-ϕ plot is the start time of that frame.

The particle energy values are displayed on the ordinate as $\log_{10}$ of the energy in units of eV. Each frame shows 16 azimuthal sector marks on the abscissa which corresponds to the spin angle ϕ. Because the spin axis is nearly perpendicular to the ecliptic plane, the abscissa can be viewed as solar ecliptic longitude, from 0 (or 360) degrees (sunward flow) to 180 degrees (antisunward flow). Angles less than 180 degrees correspond to duskward flow, and angles greater than 180 degrees correspond to dawnward flow. The detector responses are color-coded with a color bar at the right side of the color plates with values of $\log_{10}$ of the sensor response. Because the distribution function is proportional to this response multiplied by $1/E^2$, care must be taken that what often appears as a prominant bump in the E-ϕ spectrogram may actually be only a flattening in the distribution function.

III. OBSERVATIONS OF ELECTROSTATIC BURSTS AND THEIR RELATIONSHIP TO WHISTLER MODE CHORUS

A. Description Of Phenomenon

This section is devoted to a description of the electrostatic bursts observed, and their relationship to the whistler-mode chorus emissions accompanying them. A preliminary study of these relationships has been published by Reinleitner et al., [1982]. Figure 5 indicates some of the general features of this phenomenon. In the top panel at about 300 Hz is the chorus band which is often observed in the outer magnetosphere just inside of the magnetopause region. The frequency is somewhat lower than the chorus frequencies usually reported in the literature, due to the location in the outer part of the magnetosphere. The frequency is about 1/3 to 1/4 of the local electron gyrofrequency, as is usually expected for whistler mode chorus. Discrete features referred to as "hooks" by Helliwell [1965] are evident in the chorus band.

The features that are being referred to as electrostatic bursts (or simply bursts) are illustrated in the lower panel of Figure 5. They extend in a fairly broad band from about 5 kHz to about 8 kHz, and turn on and off very abruptly (on the order of ten milliseconds). In this case, the electrostatic bursts appear to be strongly correlated to the discrete features in the chorus band referred to as hooks. Most of the data shown in this section were obtained from the plasma wave instrument

on the ISEE 1 and ISEE 2 spacecraft as described in Section II. The electrostatic bursts are found to have a number of distinguishing features.

It should be noted at this point that there are two particular types of electrostatic bursts, both related to chorus. The first type is shown in Figure 5, where the bursts are of short duration, usually on the order of one second. This type of burst is usually correlated to a hook-like or other discrete feature in the chorus band. The second type is of longer duration, and is associated with an intensification of the chorus band rather than a hook-like feature. This type of burst is illustrated in Figure 6. The intensification of the chorus band in this figure is a real feature as determined by the spectrum analyzer data, and not simply a effect of the automatic gain control. The rather abrupt nature of the electrostatic bursts turning on and off with chorus band intensification, indicates that some type of threshold effect may be occurring. These long duration bursts are observed to extend from about 10 seconds to several minutes. The longer duration type of electrostatic burst was actually much more commonly observed than the type associated with the discrete hook-like feature by roughly a factor of 5 to 10, however, the shorter bursts have been very useful in the study and understanding of the entire phenomenon.

B. Wideband Characteristics

A comprehensive survey of the locations where the bursts can be observed has not yet been performed. However, all cases observed so far have been located in the Earth's outer magnetosphere near the

dayside magnetopause boundary at about 9 - 12 R_E. Cases have been found on the dayside region for many magnetic local times ranging from 7.0 to 17.5 MLT. All cases observed have been within ≈30 degrees of the magnetic equator, however this is probably due to the generally equatorial nature of the ISEE satellite orbit. Examination of the LEPEDEA data has shown that most of the observed cases are located inward from the magnetopause boundary layer. Only a few are actually located in the boundary layer region. The general region where the electrostatic bursts have been observed is indicated in Figure 1. It should be noted that for magnetosphere regions closer to the Earth than those cited, the plasma frequency tends to go above 10 kHz, which would produce electrostatic bursts at frequencies too high to be observed in this mode of the ISEE instrumentation. Thus the general limitations on the locations of the observed electrostatic bursts accompanied by chorus should be viewed as data mode limitations rather than definitive regions of occurrence.

The frequency of the bursts have always been observed to be below the local plasma frequency (f_p) as determined by the lower edge of the continuum radiation [Reinleitner et al., 1982; Gurnett and Shaw, 1973]. This difference in frequencies varies from so small as to be undetectable, to as much as 60 percent or so. The continuum radiation is sometimes rather faint, and the determination of f_p must be made from continuum radiation occurring a few minutes before or after the electrostatic burst event being displayed. The burst frequency was always well above the local electron gyrofrequency as determined by the magnetometer data [Russell, 1978] ($f_g \approx 1.2$ kHz in Figure 5). The bursts always occur as a frequency band, as opposed to a sharp monochromatic

frequency. This band is usually a few hundred Hz to several kHz in width as shown in Figures 5 and 6.

The bursts have been described as electrostatic because no wave magnetic field has been detected in association with them. This conclusion is illustrated in Figure 7, where the data from ISEE 1 are shown in the upper two panels. These data were taken with the wideband receiver connected to the electric dipole antenna. The bottom two panels from the same time period were taken with ISEE 2 where the wideband receiver was connected to the magnetic search coil antenna. As can be seen, there is a good correlation between the chorus features in the 0 to 1 kHz frequency range at both spacecraft, but no bursts seem to appear in the 0 to 10 kHz frequency range when the antenna is connected to the magnetic search coil. While the chorus is an electromagnetic mode, the bursts do not have a detectable magnetic component. Typically the broadband electric field strength of the bursts is on the order of 50 μV/m. Because the wave magnetic field remains at the instrument noise level in all cases observed, a limit can be placed on the magnetic-to-electric field ratio of about $cB/E \lesssim 4$, which corresponds to an index of refraction $n \lesssim 4$. Because no electromagnetic plasma wave mode is known to exist with $cB/E \lesssim 4$ in the frequency range $f_g < f_{burst} < f_p$, the bursts are almost certainly electrostatic. The typical field strengths of the chorus emissions associated with the electrostatic bursts are about 300 μV/m and 40 milligammas (1 gamma = 10^{-9} Tesla).

Serious consideration was given as to the possibility that the electrostatic bursts were an instrumental effect. It was felt that the

frequent occurrence of the bursts, whether accompanied by hooks in the chorus band, or simply by an intensification in the chorus band, as well as the limited physical region of occurance strongly indicate that the bursts could not be an instrumental effect. To check that the bursts are not due to some cross-modulation effect in the instrument electronics, wideband data from a completely different instrument on the IMP 6 spacecraft have been examined. Although IMP 6 was not in the correct wideband mode to observe both frequencies of interest as often as ISEE 1, electrostatic bursts of both the hook-related and long chorus intensification types have, nevertheless, been found in several passes through the outer magnetosphere on the dayside region. Examples of both types of IMP 6 observations are shown in Figures 8 and 9. In addition, the good correlation with LEPEDEA electron data shown in Section V also indicates that the electrostatic bursts accompanying the chorus are not due to an instrumental effect on the spacecraft.

The electrostatic bursts occasionally have narrowband harmonic structure of the type shown in Figure 10. The harmonic structure should not be confused with the vertical striations due to the rapid time dependence of the bursts. The harmonic structure is only evident when the chorus emission has a narrow bandwidth, such as when the hook-shaped features occur. The frequency spacing of the harmonic structure corresponds to the instantaneous emission frequency of the chorus burst. This feature will be discussed again later in this section.

When chorus hooks are found to be correlated with the electrostatic bursts, the onset of the electrostatic burst usually coincides with the minimum frequency of the hook. This may be due to the chorus having the

greatest intensity at about the minimum in the hook feature, or due to the rising frequency of the hook after the minimum. It should be noted that the electrostatic burst usually continues for a time after the hook has disappeared or merged back into the chorus band.

C. Spectrum Analyzer Measurements

It is desirable to determine all characteristics of the electrostatic burst under the assumption that it is a normal mode of the plasma. Comparative studies using both the ISEE 1 and ISEE 2 electric field multichannel spectrum analyzers have been used to determine the wave length of the bursts. Figure 11 shows an example of the electric field spectrums obtained simultaneously for a long burst that was observed in the wideband data by both ISEE 1 and ISEE 2. These spectrums indicate, when corrected for the antenna length from each spacecraft, that the electric field strength for both the chorus and the electrostatic bursts is the same at both spacecraft even with different antenna lengths. This result is expected for the chorus because the chorus wavelength is on the order of 100 kilometers and thus much greater than the length of either antenna. If the wavelength were between the two antenna lengths, then the larger antenna would detect a reduced electric field because the wavelength is shorter than the longer antenna. If the wavelength were shorter than both antennas then multilobed antenna pattern effects recurring at one half of the spacecraft spin period should appear. The fact that the electrostatic burst shows the same electric field strength at both spacecraft indicates that the wavelength of the burst must also be greater than the length of either

of the antennas. Thus the wavelength of the electrostatic bursts must be longer than the ISEE 1 electric dipole antenna so we can conclude that $\lambda_{burst} > 215$ meters.

In addition, studies of the wideband data show that although there is a good correlation between chorus hooks in both ISEE 1 and ISEE 2 data, there is only moderate correlation between the electrostatic bursts. There is a strong correlation between the burst appearance, which is probably due to the correlation between the bursts and the chorus itself. However there is not a good correlation between the structure of the individual elements of the bursts at the two satellite locations. This indicates that the wavelength of the bursts is shorter than the distance between the two spacecraft. Thus we can say that $215 \text{ m} \lesssim \lambda_{burst} < 100$ km.

The rapid sample data has also been useful to determine properties of the electrostatic bursts. In a case where the channel of the multichannel electric spectrum analyzer on ISEE 1 was set at about the frequency of the electrostatic burst, and was also in the rapid sample mode, a study of the wave polarization was possible. An example of this type of polarization analysis is shown in Figure 12, which shows that the electric field of the bursts appears to be aligned with the projection of the ambient magnetic field in the spin plane of the spacecraft. This result indicates that the electrostatic bursts have a wave vector generally aligned along the magnetic field. It should be noted here that even though the long bursts in the wideband data do not show this spin modulation effect because of the AGC, several checks of the spectrum analyzer data show that the spin modulation usually occurs.

D. Waveform Data Analysis

Since the wideband data is transmitted from the satellite in analog form and is spectrum analyzed on the ground, it is possible to study the actual waveform as seen on the electric field antenna by the spacecraft. One example is shown in Figure 13. In the lower panel of Figure 13, the electric field versus time oscilloscope waveform pattern for both the chorus and electrostatic burst is shown for the very short burst in the middle panel. The lower signal is the chorus waveform while the upper high frequency signal is the associated electrostatic burst. Both signals have been processed by bandpass filters to eliminate signals not in the frequency band of interest. Note that the time duration of these waveform data is only 8 milliseconds. The waveform therefore comprises only a small portion of the electrostatic burst from which it was taken. As can be seen, the electrostatic noise is actually composed of many shorter bursts of a high frequency signal which is modulated at the chorus frequency. Thus, the harmonics evident in Figure 10 are a modulation effect caused by the periodic modulation of the electrostatic noise at the frequency of the chorus emission. In the cases where harmonics are not observed, the electrostatic burst occurs as a frequency band, which tends to blend any harmonics into the broad continuous spectrum. It is also noted that for the long electrostatic bursts, the modulation effect is either not as strong or nonexistent. This effect is shown in Figure 14, which shows an example in 14A and 14B of a good modulation effect on a short burst associated with a hook. In Figure 14C and 14D a longer burst of about 6 seconds duration shows a much reduced modulation effect. Figure 15A and 15B show a longer burst

with a limited modulation effect, and Figure 15C and 15D show a case with no modulation effect at all. The case of Figure 15C and 15D was a little unusual in that the electrostatic bursts were much more narrow-band and closer to the electron plasma frequency than usual. Due to possible phase shifting effects in the filters used for the waveform analysis and other possible phase shifts related to the wave normal angle which is unknown, nothing can be said at this point about the absolute phase relationship between the chorus waveform and the modulated electrostatic burst.

To sum up some of the characteristics covered in this section, we have noted that electrostatic bursts appear to accompany chorus "hooks" and simple chorus intensifications in the Earth's outer magnetosphere. These bursts seem to have a wavelength such that 215 m $\lesssim \lambda_{burst} <$ 100 km. The electric field vector of the electrostatic bursts is aligned along the ambient magnetic field line, and thus the wave vector appears to be generally also aligned along the magnetic field line. Examination of the waveforms for both the chorus and bursts indicate that often the higher frequency waveform for the burst is modulated by the chorus waveform. The strong correlation between the envelope of the electrostatic bursts and the chorus suggests some strong physical interaction between these two wave modes.

IV. MODEL INTERPRETATION OF OBSERVATIONAL DATA

A. General Outline Of the Model

In the previous section, the observations of the electrostatic bursts accompanied by whistler mode chorus were described. This section describes a model that explains the observations. The most obvious characteristic of the bursts is that they are electrostatic and near the electron plasma frequency. This could suggest some form of Langmuir oscillation. However, the observed frequency occurrence at below the electron plasma frequency requires some explanation because the Langmuir oscillation always occurs at frequencies near or slightly above the electron plasma frequency. Because the wave vector for the bursts is apparently aligned in the general direction of the ambient magnetic field, the observations suggest a two-stream instability with a field-aligned beam.

The general model that is proposed is illustrated in Figure 16. It is well known that whistler mode chorus in the magnetosphere has a wave normal vector that is typically not aligned along the magnetic field lines [Burton and Holzer, 1974], although there is some question about the magnitude of the angle θ between the $\vec{k}$ vector and the $\vec{B}_o$ field in the region of interest [Burton and Holzer, 1974; Burtis and Helliwell, 1976]. In the top part of Figure 16, it is shown that when the angle θ is non-zero, the electric field of the chorus wave will have a component

$\vec{E}_{\parallel}$ along the $\vec{B}_o$ field. The actual magnitude of this $\vec{E}_{\parallel}$ is derived in Appendix B. Because the ambient magnetic field $\vec{B}_o$ in the region of interest is on the order of 40 gammas, and the wave magnetic field of the chorus is on the order of 40 milligammas, it is expected that the first order motion of the electrons will be the usual helical motion along the ambient magnetic field line.

The model, as proposed, assumes that the electrons are free to move along the ambient magnetic field line ($\vec{B}_o$), under the parallel electric field ($\vec{E}_{\parallel}$) influence of the chorus wave. The perpendicular component of the chorus wave electric field will not influence the electron motion along $\vec{B}_o$, but would at most move the electrons slightly across the field lines. Thus the electrons will only be affected by an effective potential due to $\vec{E}_{\parallel}$ along the field line such as that shown in the middle part of Figure 16. This electric field permits electrons to be trapped in effective potential wells of the chorus wave, and be carried along with the chorus wave at the chorus phase velocity.

These trapped electrons will move in bunches at the chorus phase velocity in the effective potential wells, and to a stationary observer would pass by in a periodic manner with the chorus wave. Because the trapped electrons will move at the same velocity, these electrons effectively have a delta function velocity distribution, and would therefore be expected to excite Langmuir waves via a two-stream like mechanism. The bursts of Langmuir waves would then be expected to have the modulated characteristics of the short electrostatic bursts as shown in the bottom part of Figure 16.

B. Parameters of the Model

For the characteristics of the region of interest, the index of refraction for the whistler mode is on the order of 10 to 20. This implies a phase velocity of less than one tenth the velocity of light, and with the known frequency, can be used to estimate the voltage depth of any possible potential well. A simple calculation (assuming n=10 and f = 300 Hz) gives:

$$\lambda = V_p/f$$

$$\lambda \approx 100 \text{ km}$$

This estimate implies that for a chorus wave with an electric field intensity of about 300 μV/m such as reported in Section II, the largest possible potential well would be 100 km x 300 μV/m = 30 volts. Thus the potential well for such a typical chorus wave would be less than about 30 volts. This value is encouraging, as it is large enough to be a significant potential to electrons moving at the chorus phase velocity. With an index of refraction of about 10 or 20, the electrons moving at the chorus phase velocity will have an energy of ≈ 2 keV or less.

C. Electron Trapping at the Landau Resonance

It is only recently that considerable effort has been put forth to study the possibility of particle trapping in Landau resonance (m = 0 in Equation 1) with chorus waves. Early work on resonances such as Kennel and Petchek [1966] concentrated on studies of electrons in cyclotron resonance with chorus waves (m = 1, 2, ... in Equation 1). More recent

work on Landau type of trapping has dealt with trapping in electrostatic waves by Nunn [1971; 1973]. A recent work by Inan and Tkalcevic [1982] deals with the nonlinear equations of motion for particles in Landau resonance with chorus waves. The work of Inan and Tkalcevic [1982] is greatly extended in a Doctoral Dissertation by S. Tkalcevic [1982], in which the Landau resonant trapping properties of whistler mode waves are explored. His computer model simulations yield highly interesting results and conclusions, which include the finding that there is a lower intensity threshold, below which trapping is not possible. Above this threshold trapping is possible. This threshold varies with different parameters, most notably the wave vector angle θ from the $\vec{B}_o$ field, but is in general on the order of 20 μV/m. In all cases of the observation of electrostatic bursts, the chorus intensity was well above this threshold, usually on the order of 300 μV/m.

To test the trapping of electrons at the Landau resonance for the specific parameters relevant to this study, a computer simulation was done by solving the cold plasma dispersion relation for whistler mode waves propagating at an angle to the $\vec{B}_o$ field. The resulting wave electric and magnetic fields were simulated for an electron moving with a velocity close to the Landau resonant velocity. Using a fourth order Runge Kutta solution to the equation of motion of an electron in such fields showed, as in Figure 17, that electron trapping is possible.

Figure 17 shows three examples of the phase of the electron motion for different wave vector angles θ. In each example (identical plasma parameters), $V_p/\cos\theta$ is the projected wave phase velocity along the ambient magnetic field ($\vec{B}_o$), V_z is an arbitrarily set particle initial

velocity along $\vec{B}_o$, and ΔE is the energy difference between an electron moving at $V_p/\cos\theta$ and one moving at V_z. The simulation was done using a box one wavelength long along the wave vector direction with periodic boundary conditions. Z-phase is the relative phase between the electron position and the wave front. Trapping is defined as the point in time when the phase variation of z-phase becomes bounded. In the simulation the chorus wave electric field amplitude (E_o) is allowed to grow linearly with time and trapping occurs when E_o becomes large enough to produce bounded oscillatory motion (on the order of 40 - 80 μV/m). The results obtained show that the required E_o for trapping decreases as the wave vector angle θ increases. The equations and work on this simulation are given in Appendix B.

It should be noted that this solution was a rather brute force one of following the particle step-by-step for a step size of much less than the gyroperiod of the particle. The more extensive work done by Tkalcevic [1982] was accomplished in a more computationally elegant way by analytically solving the nonlinear equations of motion and averaging over an entire gyroperiod [Inan and Tkalcevic, 1982]. This reduced the total computer time requirements greatly. The simulation in Appendix B shows particle trapping at electric field intensities that are consistent with those found in Tkalcevic [1982], as seen in Figure 17.

Consideration as to possible methods of obtaining the modulated burst appearance other than trapping were studied. The possibility of electrons being simply repetitively accelerated and decelerated in the electric field of the chorus wave was considered, but the energy gain would be limited to about 30 eV as in the potential well calculation.

This gain would be insufficient to produce a two-stream instability. Trapping was the only viable method left to explain the well modulated nature of the short electrostatic bursts.

Electrons may be trapped into the potential wells by at least two possible mechanisms. In one case the chorus wave amplitude may simply increase with time, thereby trapping electrons with velocities close to the chorus phase velocity, as was done in the particle simulation described. In another case the chorus wave phase velocity may be increasing, and as the phase velocity matches the velocity of new electrons these electrons are trapped in the potential wells.

Electrons may also be detrapped by several possible mechanisms. Mutual electrostatic repulsion due to too many trapped electrons could push some of the electrons out of the potential well (Poisson's equation was ignored for the simulation). The chorus wave may accelerate in phase velocity at so great a rate as to dump or "slosh" them out of the potential wells. Furthermore, as the wave propagates into regions of stronger magnetic field, the magnetic moment force $-\mu\ \partial B/\partial z$, can become large enough to detrap the electrons. Any of these detrapping mechanisms could explain the observed saturation in burst amplitudes in Figure 14.

Trapping alone would probably not explain enough electron enhancement at the chorus phase velocity to create something like a two-stream bump-on-tail instability, since trapped electrons oscillating in the potential well still have the same range of velocity as before trapping occurs. Some mechanism is required to translate these electrons into a region of velocity space with a lower phase space density, so that a

double-humped velocity distribution is produced. A likely candidate is some form of acceleration of a growing chorus wave, which both traps and simultaneously accelerates the trapped electrons. This process is illustrated in Figure 18, where a chorus wave moves from the equatorial regions, roughly following the magnetic field lines. As the chorus wave moves to higher latitudes, the $\vec{B}_o$ field increases, decreasing the index of refraction, and causing an increase in phase velocity of the chorus wave, which in turn would accelerate any electrons that were trapped at the chorus phase velocity. This would, of course, be in competition with the tendency of the index of refraction to increase due to increasing plasma density at higher latitudes. With the high electron temperature in the region, it is not clear which trend would dominate. Another possible acceleration mechanism is made clearer by studying the case of hooks. The electrostatic burst usually seems to be associated with the rising portion of the chorus. As the chorus frequency rises, the index of refraction decreases, increasing the phase velocity. This could be another possible acceleration mechanism.

The exact method of electron acceleration to create a positive slope in the distribution function is not considered to be an integral part of the model described here. Some gain in velocity for certain electrons is, however, required. The effect of this electron acceleration is to move part of the distribution function up to higher velocities, thereby creating a bump in the new distribution function. Only a small increase in velocity would be necessary if the trapped electrons have a sufficiently narrow velocity width, and the bump sufficiently approximated a delta function, for a two-stream instability to arise.

V. RESULTS FROM LEPEDEA DATA

A. Search For Electron "Beam"

The most obvious feature predicted by the model described in Section IV is the existance of the enhanced trapped electrons which should be moving at the phase velocity of the chorus wave. Knowing the plasma frequency from the continuum radiation, the $\vec{B}_o$ field from the Data Pool tape using the ISEE 1 Fluxgate Magnetometer experiment described by Russell [1978], and the chorus frequency as obtained from the wideband data, it is possible to determine the phase velocity of the whistler mode wave. The only unknown parameter is the wave normal angle θ. The phase velocity is however, only weakly dependent upon θ, unless θ approaches the resonance cone angle. Using the theoretical value of the phase velocity, a search for an electron beam aligned along the $\vec{B}_o$ field was performed using the LEPEDEA instrument on ISEE 1.

There are some difficulties in using particle data to search for this electron beam. The main limitation in the LEPEDEA instrument for this purpose is the time required for a full energy scan. An entire three dimensional distribution function requires 128 seconds when the satellite is in the high bit rate mode, while most electrostatic bursts are much shorter than a two minute duration. Short bursts accompanying chorus hooks are simply not possible to observe with the LEPEDEA data. A careful study was made of the ISEE 1 wideband data to find some cases

of bursts long enough for a study of the LEPEDEA data to be useful. Ten possibilities were found where either one long electrostatic burst, or several shorter electrostatic bursts covered at least 70% of a two-minute period in the wideband data. These possibilities were checked with detailed computer listings of the LEPEDEA instrument responses. It was anticipated that some of these cases would not detect a beam due to several factors. Since only one short sample period of the 128 second energy scan will be at the correct energy to detect the beam, there is a possibility that the burst would not be occurring at the appropriate sample time. In addition, the plasma density in the outer magnetosphere is usually very low, typically less than 1 electron/cm^3, so that plasma analyzers often obtain poor statistical sample rates in this region. Out of the ten selected cases, there were three that showed no clear sign of any field-aligned enhancement, and seven that showed some detection of an electron enhancement. Due to limitations of computer time only the two best cases in the instrument response listings were converted into E-ϕ spectrograms. These two cases are shown in Figures 19 and 20.

In both of these E-ϕ spectrogram events the detectors 2 and 6 are the detectors that will point along the ambient magnetic field line as determined from the orientation of the spacecraft and the magnetic field data from the magnetometer experiment [Russell, 1978]. From the magnetometer data used, the angle ϕ for the enhancement shown in both figures corresponds to that of the field line. Thus, the enhancements are field-aligned, which is the expected direction for a beam in Landau resonance with the chorus.

B. Characteristics of Electron "Beams"

One clear feature that emerges from Figures 19 and 20 is that there are actually two counterstreaming electron enhancements at the same energy. This effect is easily understood if the bounce time for a mirroring particle is examined. From Van Allen [1961], an equation for the bounce time of a trapped electron in the Earth's geomagnetic field is given by:

$$\tau_2 = 0.85(r_o/\beta)\ T(\alpha_o) \text{ seconds} \qquad (3)$$

In this equation r_o is in Earth radii, β is v/c, $T(\alpha_o)$ is a parameter ranging from about 0.56 to 1.3. Thus the bounce period for $r_o \approx 10\ R_E$, $\beta \approx 1/10$, and $T(\alpha_o) \approx 1$ is $\tau_2 = 8.5$ seconds. This bounce time is not exactly correct as the derivation was for a dipolar field, but it shows that the bounce period is on the order of 10 seconds. Thus for long bursts, such as the ones examined by the LEPEDEA instrument, the electrons will be mirroring back and forth along the field line and will show up in the LEPEDEA data as two counterstreaming electron enhancements.

It is also worth noting here that the LEPEDEA instrument is not expected to temporarily resolve the modulated or periodic nature of the electron enhancements. The instrument averages over the 0.25 second sample interval. It is expected that for the long bursts, the spatial bunching of the electrons is no longer occuring. In the waveform studies of the long bursts, the modulation effect is not very dominant and is often completely absent. It is thus a very strong possibility that

any electron trapping and acceleration may be occuring at some other location along the field line, and that the electron enhancements observed by LEPEDEA instrumentation are no longer moving at the local chorus phase velocity.

For the case in Figure 19, on day 222/79, the following plasma characteristics were noted:

$f_p \approx 5.7$ kHz

$f_{chorus} \approx 150$ Hz

$\vec{B}_o = 25.1$ gamma

These parameters yielded a value for the index of refraction of 19.8, which would correspond to an electron moving with an energy of 650 eV (±40%), while the center of the enhancement in Figure 19 is at 630 eV (±20%). This close agreement must probably be regarded as somewhat fortuitious, since for the second case in Figure 20, on day 263/80, the agreement is not as good. The plasma parameters for the second case are:

$f_p \approx 6.5$ kHz

$f_{chorus} \approx 400$ Hz

$\vec{B}_o = 30.8$ gamma

These parameters yield a value for the index of refraction of 15.1, which would correspond to an electron moving with an energy of 1120 eV (±30%), while the center of the enhancement in Figure 20 is at 400 eV (±20%). Because the local chorus phase velocity and the beam velocity differ by a significant amount ($V \propto \sqrt{\text{Energy}}$), it is thought that the

acceleration of the ≈ 400 eV electrons is taking place somewhere else along the $\vec{B}_o$ field line. In this case, the beam electrons may have been accelerated by a change in the chorus phase velocity before escaping from the potential well through one of the mechanisms described in Section IV.

Both of the cases shown in Figures 19 and 20 were found to have the electron enhancements appear in the E-ϕ spectrograms when the long duration burst appeared, and to persist for several minutes afterward, fading out gradually, rather than abruptly turning off as the electrostatic burst does. The case of day 263/80 is shown in Figures 21 and 22. Figure 21 shows a standard case of wideband data from ISEE 1 For September 19-20, 1980. In this figure the chorus shows up clearly as a dark band in the upper panel at about 300 Hz. The electrostatic burst shows up clearly as a dark band in the lower panel from about 3.5 - 7.0 kHz. The fact that the continuum radiation from about 6.5 kHz up to the top of the bottom panel ceases when the burst appears is an effect of the automatic gain control, since the burst is of much greater intensity than the continuum radiation. The time scale is much lower resolution than the other wideband figures in this work, and covers a period of 10 minutes with the 2 1/2 minute electrostatic burst labeled at its start time with an A, and its end time with a B. There is a long period after the end of the burst with little or no chorus and burst activity.

Figure 22 shows a time series of E-ϕ spectrogram panels for the same time period as Figure 21. Only detectors 2E and 6E are important in this time period as they show the counterstreaming beam very clearly. As recalled from Section II, time as well as energy is given on the

ordinate of each detector panel, with a time of ≈ 128 seconds per panel. The start times of each panel are given between the corresponding detector panels, and an A for the start time of the burst, as well as a B for the end time of the burst is given for each detector. As can be seen, the field-aligned electron enhancement is strongest during the burst, and gradually fades away. The strong relationship between the simultaneously occuring chorus and burst, and the field-aligned electron enhancements or "beams" seems from this figure to be very clear. This gradual fading out of the counterstreaming beams would also seem to be an effect of the mirroring electrons bounding back and forth between their conjugate mirror points several times before being lost.

A perspective plot showing the entire electron distribution function for a 128 second event on day 222 in 1979 is shown in Figure 23. This corresponds to the same event as that shown in Figure 19. This perspective plot clearly shows the field-aligned enhancements. By integrating over just the enhancement and subtracting the distribution without the enhancement, a value for the beam density can be obtained. This integration was performed using the data that generated the perspective plot, and not the perspective plot itself. The value of the beam density divided by the plasma density was 2.5×10^{-3} for the positive $V_{\parallel}$ enhancement, and 1.3×10^{-3} for the negative $V_{\parallel}$ enhancement. If there is a cold electron component to the plasma that is not detected by the LEPEDEA instrument, then these values would have to be lowered. From the plasma density values given from the continuum radiation in the wideband data, these values would have to be lowered by about a factor

of two. The electron field-aligned enhancements seem thus to be about three orders of magnitude less than the plasma density.

If an energy gain of about 30 eV is assumed for each electron in the enhancement, and the chorus wave is assumed to have a magnetic field intensity of approximately 40 milligamma, the wave energy density of the chorus is approximately the energy gain per unit volume for the electron enhancement. Most of the chorus wave energy resides in the magnetic field. Thus, the chorus wave energy would only have to be twice the observed value initially to create the electron beam. The electric field energy density of the electrostatic burst is about three orders of magnitude less than the energy density of the chorus wave if the value of 50 μV/m is used. Thus, energy considerations for the model outlined in Section IV would appear to be satisfied.

VI. THE THEORY OF THE RESISTIVE-MEDIUM INSTABILITY AND ITS COMPARISON TO OBSERVATIONS

A. Difficulties with Simple Beam Theory

The standard simple two-stream theory, as is described in most introductory plasma physics texts such as Krall and Trivelpiece [1973], is not adequate to describe the observations of the electrostatic bursts. The primary difficulty with the theory is that for a weak beam the frequency with the maximum growth rate is predicted to be at the electron plasma frequency, $\omega = \omega_{pe}$, whereas the bursts usually occur below this frequency.

A slight improvement is obtained by considering a finite beam density, as in Equations 1.51 and 1.52 from Mikhailovskii [1970]. This simple derivation assumes a finite but small beam density represented by the parameter $\alpha << 1$ where $\alpha = n_b/n_e$, and n_b is the beam density, n_e is the plasma electron density. Using a simple Taylor expansion about $\omega^{(0)} = \omega_{pe}$, the first order corrections to the dispersion relation were obtained with the result that the frequency and growth rate are given by

$$\text{Re } \omega = \omega_{pe}\left[1 - \frac{\alpha}{(2)^{4/3}}^{1/3}\right] \tag{4}$$

and

$$\text{Im } \omega = \omega_{pe} \frac{\sqrt{3}}{(2)^{4/3}} \alpha^{1/3} \tag{5}$$

It is noted that this finite beam approximation provides a reasonable growth rate for the instability, and a reduction in the real frequency of the oscillation below the plasma frequency. The reduction in frequency is, however, not sufficient to explain the large (60%) reductions sometimes observed for the electrostatic bursts, unless a totally unreasonable beam density is assumed ($\alpha \approx 1$). A large beam density would likewise invalidate the assumption that $\alpha << 1$, which was made for the derivation. In Section V, it was shown that the LEPEDEA data yielded $\alpha \approx 10^{-3}$.

B. Resistive-Medium Instability

A very interesting derivation of an instability that appears to explain many of the above difficulties is discussed in Briggs [1964]. This instability is called the resistive-medium instability. The derivation of this instability is outlined in Appendix A. This derivation is made for a one-dimensional system. It assumes a weak beam system with the beam and the background plasma ions being cold, but with the background electrons being warm. In this derivation, a resonance distribution was used for mathematical simplicity, which will be shown to provide a reasonable model under the conditions that exist in the magnetospheric plasma. The derivation in fact showed two different instabilities, called the reactive-medium instability and the resistive-medium instability, both of which are important under different regimes of V_o/V_T, where V_o is the "beam" velocity, and V_T is the average longitudinal thermal velocity.

The reactive-medium instability has a large growth rate when $V_o >> V_T$, and is essentially the normal bump-on-tail two-stream instability and yields results virtually identical to Equations 4 and 5. In this case, since the phase velocity of the waves excited would be near V_o and well out in the tail of the distribution function, the resonance distribution assumed would be irrelevant to the calculations. For the derivation to be valid, the distribution function used would need to be the actual distribution function in the region of the beam. This instability will diminish in importance as V_o approaches V_T since then Landau damping becomes important, and damps out the wave faster than it can grow.

The resistive-medium instability is a different type of instability which requires dissipation and occurs when V_o is on the order of V_T. This condition means that Landau damping is essential to the instability and that the beam must be on the slope of the distribution, not on the tail. In this case, the resonance distribution is a fairly good assumption. Since the reactive-medium instability will dominate in the case of $V_o >> V_T$, the resistive-medium instability will only be observed for very low velocity beams, or plasmas with very hot electrons. It is this latter case for the outer magnetosphere. As given in Section IV, the thermal velocity in the regions of interest corresponds to electron energies in the range of 200 - 600 eV. Thus for electron beams with energies from 200 eV to 2 keV, we are well in the range of the resistive-medium instability.

With use of Equations A8, A9, and A10 derived in Appendix A, we can produce a graph of the imaginary component of ω versus the real part of

ω. The entire imaginary component of ω is contained in $\delta\omega$, and from the equations it is always multiplied by ω_{pb}, the plasma frequency due to the beam alone. Thus it is a function of beam density. Figure 24 presents such a graph where ω_i is scaled by ω_{pb}, and the real frequency is scaled by ω_{pe}. Several cases of V_o/V_T are shown. From this figure it is very clearly seen that for cases where V_o/V_T is close to 1, there is a very significant downshift in the frequency for which maximum growth occurs when compared to the electron plasma frequency. This downshift below ω_{pe} is easier to understand from Figure 25 in which the frequency of maximum growth is plotted versus V_o/V_T. Since the electron beams actually observed had energies of 400 eV and 630 eV, and the thermal velocity in the outer magnetosphere corresponds to electron energies in the range of $\approx$ 200 - 600 eV, it is seen from this figure that the downshift in frequency below the plasma frequency by factors ranging from a few percent to sixty percent is easily predicted from the observed parameters.

The absolute growth rates predicted by the theory must match the growth rates shown in Figures 13, 14, and 15 for the burst waveforms. If $\omega_i \approx 1/\tau$ where τ is the time required for the envelope of a modulated burst to increase by a factor of e, then to an order of magnitude from the theory as graphed in Figure 24:

$$\frac{\omega_i}{\omega_{pb}} \approx 1 \qquad \text{(theory)}$$

From the waveforms in Figures 13, 14, and 15 we also observe that:

$$\frac{\omega_i}{\omega_{pe}} \approx 3 \times 10^{-2} \qquad \text{(experimental)}$$

This experimental value would cause the theory to predict that:

$$\frac{\omega_{pb}}{\omega_{pe}} \approx 3 \times 10^{-2}$$

which implies that:

$$\frac{n_b}{n_e} \approx \left(\frac{\omega_{pb}}{\omega_{pe}}\right)^2$$

$$\approx 9 \times 10^{-4}$$

$$\approx 10^{-3} \qquad \text{(predicted)}$$

This value predicts from the theory and the experimentally determined ω_i that the beam density should be about three orders of magnitude less than the plasma density, which is in agreement with the LEPEDEA results. Thus, the absolute growth rate predicted by the theory is of the correct magnitude as compared to the observed growth rates, and the LEPEDEA beam density results.

Another important factor was noted in the curves of Figure 24. As V_o/V_T decreases, the peak in the growth curves becomes less narrow.

This observation predicts a factor that had not been noticed in the wideband data. There is a tendency for cases of electrostatic bursts that are downshifted in frequency by a large percentage of f_p to have a wider spread in frequency band excited. This tendency is illustrated in Figure 26 which shows a large number of cases where the spread in the observed frequencies divided by the center of the burst frequency is is plotted versus the center of the burst frequency divided by the plasma frequency. In simpler terms this is just the burst frequency spread versus downshift in frequency. Figure 26 indicates that a clear correlation exists between these two observed characteristics of the electrostatic bursts.

In order to obtain some idea what the theoretical relationship between these two parameters should be, an examination is made of the range of growth rates expected to be observed in the wideband data. The range in intensity observable in the wideband data is better than 10dB. Let us assume that the amplitude of the burst at a particular frequency is dependent on the imaginary component of ω (ω_i) at that frequency. At one instant in time, the spread of frequencies observed on the wideband spectrograms will thus be all frequencies that have an amplitude within 10 dB of the central frequency of maximum amplitude. If we define ω_{max} (ω_{min}) to be the frequency of maximum (minimum) amplitude visible on the wideband data; where $A(\omega)$ is the amplitude intensity of the burst wave at frequency ω:

$$A(\omega) \propto k_1 \, e^{k_2 \omega_i(\omega)} \qquad (6)$$

and k_1 and k_2 are arbitrary constants, then:

$$\text{Power} \propto A(\omega)^2 \propto k_1^2 \, e^{2k_2\omega_i(\omega)} \tag{7}$$

and the power of the maximum intensity visible on the wideband data is:

$$P_{max} \propto A(\omega_{max})^2 \propto k_1^2 \, e^{2k_2\omega_i(\omega_{max})} \tag{8}$$

Assuming a 10 db power difference for the frequencies ω_{max} and ω_{min}:

$$P_{min} = \frac{1}{10} P_{max} = \frac{1}{10} A^2(\omega_{max}) \tag{9}$$

$$\therefore \quad 10 \, A^2(\omega_{min}) = A^2(\omega_{max}) \tag{10}$$

$$10k_1^2 \, e^{2k_2\omega_i(\omega_{min})} = k_1^2 \, e^{2k_2\omega_i(\omega_{max})} \tag{11}$$

$$\ell n \, 10 + 2k_2 \, \omega_i(\omega_{min}) = 2k_2\omega_i(\omega_{max}) \tag{12}$$

$$\therefore \quad \omega_i|_{max} = \omega_i|_{min} + \frac{1}{k_2} \, (1.15) \tag{13}$$

Thus we clearly see that the reduction in the growth rate ω_i that is visible in the wideband data, to that growth rate ω_i that is just barely

detectable in the wideband data, is a constant factor. Taking a case from Figure 24 where $\omega/\omega_{pe} = 0.85$, we observe from Figure 26, that this corresponds to a frequency spread of $f_s/f_b \approx 0.3$. In Figure 24 a dotted line indicating $f_s/f_b \approx 0.3$ (where f_s is the frequency spread of the burst, and f_b is the center frequency of the burst) is drawn on the ω_i curve for $V_o/V_T = 4.0$. Using the same ω_i reduction for the other curves, the line indicated as theory is obtained for Figure 26. This comparison shows that the observed frequency spread matches the theory extremely well in a qualitative sense. This frequency spread derivation is for a simple mono-energetic beam. If the contributing electrons are significantly spread in energy this could participate in the frequency spread.

The theory also predicts that the electrostatic bursts should be propagating waves with a phase velocity of approximately the beam velocity. If a phase velocity of 1/20 the speed of light (corresponding to a 640 eV electron beam), and a burst frequency of $\approx$ 10 kHz is assumed, this will imply $\lambda_{burst} = 1.5$ km. This wavelength is in agreement with the observationally determined limits on λ_{burst} given in Section III. The resistive-medium instability has thus been shown to display essentially all of the characteristics of the electrostatic bursts.

VII. RELEVANCE TO OTHER PHENOMENON

This study could prove useful in understanding certain phenomenon in regions other than the Earth's outer magnetosphere also. Figure 27 shows some digitally transmitted wideband data from Voyager 1 during its encounter with Saturn's magnetosphere. The region is located at 15.6 Saturnian radii on the inward bound leg of the trajectory, and thus is in the dayside of the Saturnian magnetosphere. This region corresponds approximately to the same region in the Earth's magnetosphere that the electrostatic bursts described in this study are located [W. Kurth, private communication, 1982]. The bursts of noise at about 8 kHz in the lower panel of Figure 27 is very suggestive of electrostatic bursts, having the same abrupt turn-on and turn-off, as well as harmonics at about 1/3 of the local electron gyrofrequency. Thus the harmonics observed are at about the anticipated chorus frequency, though unfortunately there is too much instrument noise at the low frequencies to identify any possible chorus. There is not conclusive proof that this phenomena is the same as the chorus related electrostatic burst described in this study, but the evidence is very suggestive.

A report was made by Kennel et al. [1980] on correlated whistler mode and electron plasma oscillation bursts in the solar wind using data from the ISEE 3 spacecraft. This spacecraft is kept in a halo orbit on the Earth-Sun line at about one hour solar wind travel time upstream

from the earth. The ISEE 3 spacecraft lacked the wideband instrumentation, and the multichannel electric and magnetic spectrum analyzers were used instead. It is thus not clear if the "electron plasma oscillations" reported were below the plasma frequency or not. The interaction between the two wave modes described in this study is regarded as a better alternative than the secondary impulsive electron heating mechanism proposed by Kennel et al. [1980] for his observations. The instability generating the electrostatic oscillations could prove to be the conventional bump-on-tail instability, instead of the resistive-medium instability. If this is the case, then the electron oscillations reported would really be at the local plasma frequency.

Another possible application of this work is to the study of x-ray microbursts in the auroral zone [Oliven and Gurnett, 1968]. Electron precipitation (> 10 keV) causing these microbursts is usually considered to be pitch angle scattered electrons associated with the generation of chorus. However, at higher magnetic latitudes Landau trapping and acceleration of electrons by whistler mode chorus itself could produce these electrons, if the chorus phase velocity is beginning to approach a significant fraction of the speed of light.

Thus, the interaction between the whistler mode chorus waves and the observed electrostatic bursts described in this study would appear to have possible relevence in a large number of space physics phenomena. Though the interaction is best understood for the region of the Earth's outer magnetosphere, the interaction could explain some features in space physics data that are not presently understood.

VIII. SUMMARY AND CONCLUSIONS

This study has shown a number of relatively new features in the wave modes at the Earth's outer magnetosphere. It has described and given the observational characteristics of a form of electrostatic burst that is strongly associated with whistler mode chorus waves in the same region. The understanding of this relationship was assisted by a simple model of electron Landau trapping and acceleration by the electromagnetic chorus wave. This simple model was supported by a computer particle simulation of an electron in a growing amplitude chorus wave, which indicated that trapping should occur. By any of several mechanisms the chorus wave phase velocity could increase, accelerating any electrons trapped in Landau resonance with the chorus wave. This would be similar to the traveling-wave linear particle accelerators used in high energy physics. Results from the LEPEDEA data showed a significant field-aligned electron enhancement or beam at approximately the chorus phase velocity when chorus waves and electrostatic bursts of long duration are observed.

A resistive-medium instability is used to describe the electrostatic burst generation by the trapped and accelerated electrons. This instability is valid where the beam velocity is on the order of the plasma electron thermal velocity, which is shown from LEPEDEA data to be the case for the region of interest. The resistive-medium instability

proved very satisfactory in explaining the frequency downshift in the bursts to well below the local plasma frequency. In addition, the theory predicted a frequency spread relationship to the frequency downshift for the burst, that is in good agreement with the observed frequency spread of the electrostatic bursts. Overall, very strong evidence is accumulated that the model of the electrostatic bursts and their interaction with whistler mode chorus is correct and that the resistive-medium instability is the generation mechanism of the bursts. A good illustration of the energy flow for this entire model is shown in Figure 28. The energy densities of the chorus waves, electron enhancements, and electrostatic bursts were shown consistent with this model and burst generation mechanism.

REFERENCES

Anderson, R. R., G. K. Parks, T. E. Eastman, D. A. Gurnett, and L. A. Frank, Plasma waves associated with energetic particles streaming into the solar wind from the Earth's bow shock, J. Geophys. Res., 86, 4493, 1981.

Brice, N., Fundamentals of very low frequency emission generation mechanisms, J. Geophys. Res., 69, 4515, 1964.

Briggs, R. J., Electron-Stream Interaction With Plasmas, Research Monograph No. 29, M.I.T. Press, Cambridge, Massachusetts, 1964.

Burtis, W. J., and R. A. Helliwell, Banded chorus - A new type of VLF radiation observed in the magnetosphere by OGO 1 and OGO 3, J. Geophys. Res., 74, 3002, 1969.

Burtis, W. J., and R. A. Helliwell, Magnetospheric chorus: Occurrence patterns and normalized frequency, Planet. Space Sci., 24, 1007, 1976.

Burton, R. K., and R. E. Holzer, The origin and propagation of chorus in the outer magnetosphere, J. Geophys. Res., 79, 1014, 1974.

Dowden, R. L., Doppler-shifted cyclotron radiation from electrons: A theory of very low frequency emissions from the exosphere, J. Geophys. Res., 67, 1745, 1962.

Eastman, T. E., and L. A. Frank, Observations of high-speed plasma flow near the Earth's magnetopause: Evidence for reconnection?, J. Geophys. Res., 87, 2187, 1982.

Frank, L. A., D. M. Yeager, H. D. Owens, K. L. Ackerson, and M. R. English, Quadrispherical LEPEDEAS for ISEE's-1 and -2 plasma wave measurements, IEEE Trans. Geosci. Electron., GE-16, 221, 1978a.

Frank, L. A., K. L. Ackerson, R. J. DeCoster, and B. G. Burek, Three-dimensional plasma measurements within the earth's magnetosphere, Space Sci. Rev., 22, 739, 1978b.

Gurnett, D. A., and R. R. Shaw, Electromagnetic radiation trapped in the magnetosphere above the plasma frequency, J. Geophys. Res., 78, 8136, 1973.

Gurnett, D. A., F. L. Scarf, R. W. Fredricks, and E. J. Smith, The ISEE-1 and ISEE-2 plasma wave investigation, IEEE Trans. Geosci. Electron., GE-16, 225, 1978.

Helliwell, R. A., Whistlers and Related Ionospheric Phenomena, Stanford University Press, 1965.

Helliwell, R. A., A theory of discrete VLF emissions from the magnetosphere, J. Geophys. Res., 72, 4773, 1967.

Helliwell, R. A., and J. P. Katsufrakis, VLF wave injection into the magnetosphere from Siple Station, Antarctica, J. Geophys. Res., 79, 2511, 1974.

Helliwell, R. A., and U. S. Inan, VLF wave growth and discrete emission triggering in the magnetosphre: A feedback model, J. Geophys. Res., 87, 3537, 1982.

Inan, U. S., and S. Tkalcevic, Nonlinear equations of motion for landau resonance interactions with a whistler mode wave, J. Geophys. Res., 87, 2363, 1982.

Kennel, C. F., and H. E. Petschek, Limit on stably trapped particle fluxes, J. Geophy. Res., 71, 1, 1966.

Kennel, C. F., F. L. Scarf, F. V. Coroniti, R. W. Fredricks, D. A. Gurnett, and E. J. Smith, Correlated whistler and electron plasma oscillation bursts detected on ISEE 3, Geophys. Res. Lett., 7, 129, 1980.

Kennel, C. F., and R. M. Thorne, Unstable growth of unducted whistlers propagating at an angle to the geomagnetic field, J. Geophys. Res., 72, 871, 1967.

Koons, H. C., The role of hiss in magnetospheric chorus emissions, J. Geophys. Res., 86, 6745, 1981.

Krall, N. A., and A. W. Trivelpiece, Principles of Plasma Physics, McGraw-Hill, 1973.

Luette, J. P., C. G. Park, and R. A. Helliwell, Longitudinal variations of very low frequency chorus activity in the magnetosphere: Evidence of excitation by electric power transmission lines, Geophys. Res. Lett., 4, 275, 1977.

Mikhailovskii, A. B., Theory of Plasma Instabilities (Volume 1: Instabilities of a Homogeneous Plasma), Consultants Bureau, New York - London, 1974.

Nunn, D., Wave particle interaction in electrostatic waves in an inhomogeneous medium, J. Plasma Phys., 6, 291, 1971.

Nunn, D., The sideband instability of electrostatic waves in an inhomogeneous medium, Planet. Space Sci., 21, 67, 1973.

Oliven, M. N., and D. A. Gurnett, Microburst phenomena 3. An association between microbursts and VLF chorus, J. Geophys. Res., 73, 2355, 1968.

Reinleitner, L. A., D. A. Gurnett, and D. L. Gallagher, Chorus-related electrostatic bursts in the Earth's outer magnetosphere, Nature, 295, 46, 1982.

Rosenberg, T. J., R. A. Helliwell, and J. P. Katsufrakis, Electron precipitation associated with discrete very-low-frequency emissions, J. Geophys. Res., 76, 8445, 1971.

Russell, C. T., The ISEE 1 and 2 fluxgate magnetometers, IEEE Trans. Geosci. Electron., GE-16, 239, 1978.

Stix, T. H., The Theory of Plasma Waves, McGraw-Hill, New York, N.Y., 1962.

Tkalcevic, S., Nonlinear Longitudinal Resonance Interaction of Energetic Charged Particles and VLF Waves in the Magnetosphere, Ph.D. Dissertation, Stanford University, 1982.

Tsurutani, B. T., and E. J. Smith, Postmidnight chorus: A substorm phenomenon, J. Geophys. Res., 79, 118, 1974.

Van Allen, J. A., Dynamics, composition and origin of the geomagnetically-trapped corpuscular radiation, Transactions of the International Astronomical Union, 11B, 99, 1962.

APPENDIX A:

DERIVATION OF RESISTIVE-MEDIUM INSTABILITY EQUATIONS

This derivation is very similar to that derived in Briggs [1964]. The derivation is made for a one-dimensional system and utilizes a dispersion relation for a weak electron beam ($n_b << n_e$) through a plasma, where both the electron beam and the plasma ions are cold. The background plasma electrons are warm, however. The dispersion relation for such a system is given in Briggs [1964] as:

$$\frac{\omega_{pb}^2}{(\omega - kV_o)} = K_{\parallel}(\omega,k) \tag{A1}$$

and

$$K_{\parallel}(\omega,k) = 1 - \frac{\omega_{pi}^2}{\omega^2} - \omega_{pe}^2 \int \frac{f_{oe}(v_z)dv_z}{(\omega - k\, v_z)^2} \tag{A2}$$

where: $K_{\parallel}(\omega,k)$ = longitudinal dielectric constant of the plasma in the absence of the beam.

ω = the frequency.

k = the wavevector magnitude.

V_o = the beam velocity.

$\omega_{pe}(\omega_{pi})$ = the electron(ion) plasma frequency.

ω_{pb} = the plasma frequency due only to the electron beam.

f_{oe} = the electron distribution function for the warm plasma electrons.

For mathematical simplicity, a resonance distribution function for the electrons is assumed to be of the form:

$$f_{oe}(V_z) = \frac{V_T}{\pi}\left(\frac{1}{v_z^2 + V_T^2}\right) \tag{A3}$$

where V_T is the average longitudinal thermal velocity.

The integral in Equation A1 can be solved by taking a contour in the upper half of the complex V_z plane and the result is

$$\omega_{pe}\int \frac{f_{oe}(v_z)dv_z}{(\omega - kv_z)^2} = \frac{\omega_{pe}}{(\omega - i\,kV_T)^2}$$

Thus Equation A2 becomes:

$$K_{\parallel}(\omega,k) = 1 - \frac{\omega_{pi}^2}{\omega^2} - \frac{\omega_{pe}^2}{(\omega - i\,kV_T)^2} \tag{A4}$$

Now the solution for beam waves from Equation A1 is obtained only where $\omega \approx kV_o$. Thus, Equation A1 will be rewritten using:

$$\omega - kV_o = \delta\omega(k) \tag{A5}$$

where $\delta\omega \ll kV_o$. In this derivation $\delta\omega(k)$ is considered to be a "correction" in ω at some real k because of the small beam density. It

should be noted that the entire imaginary component of ω, forming both damping and growth, is contained in the $\delta\omega$ term. Since $\delta\omega$ is a small correction we can Taylor expand Equation A1 around $\omega = kV_o$ and obtain:

$$\frac{\omega_{pb}^2}{\delta\omega^2} = k_{\parallel}(\omega = kV_o) + \delta\omega\left(\frac{\partial K_{\parallel}}{\partial\omega}\right)_{\omega=kV_o} \tag{A6}$$

Now in general:

$$K_{\parallel}(\omega = kV_o) = K_R + i\,K_I$$

where the imaginary part of $K_{\parallel}$ arises from Landau damping. An instability will occur whenever a complex $\delta\omega$ with $\mathrm{Im}(\delta\omega) < 0$ arises from Equation A6. There are two basic mechanisms as described in Briggs [1964] that can cause instabilities. These are referred to as the reactive-medium instability and the resistive-medium instability.

The reactive-medium instability will occur if $V_o >> V_T$, such that Landau damping can be neglected. This will imply that K_I is vanishingly small and may be neglected in the solution of Equation A6. The solution obtained in this case will be essentially the usual dispersion relation for Langmuir oscillations of the two-stream instability.

Of great interest to this work is the resistive-medium instability. This instability is derived from Equation A6 when $V_o \approx O(V_T)$. When V_o is on the order of V_T, K_I is not a vanishing small term, and indeed

Landau damping will dominate the last term in Equation A6. The novel feature in the resistive-medium instability is that it requires Landau damping to obtain wave growth. If the final term is neglected in Equation A6 we obtain (using Equation A4):

$$\frac{\omega_{pb}}{\delta\omega^2} = K_{\parallel}(\omega = kV_o)$$

$$= 1 - \frac{\omega_{pi}^2}{\omega^2} - \frac{\omega_{pe}^2}{(\omega - i\,kV_T)^2}\Bigg|_{\omega=kV_o}$$

$$= 1 - \frac{\omega_{pi}^2}{\omega^2} - \frac{\omega_{pe}^2}{\omega^2(1 - i\frac{V_T}{V_o})^2}$$

which implies:

$$\delta\omega^2 = \omega_{pb}^2\left[1 - \frac{\omega_{pi}^2}{\omega^2} - \frac{\omega_{pe}^2}{\omega^2(1 - i\frac{V_T}{V_o})^2}\right]^{-1} \tag{A7}$$

$$= \omega_{pb}^2\left[\frac{\omega^2(1 - i\frac{V_T}{V_o})^2 - \omega_{pi}^2(1 - i\frac{V_T}{V_o})^2 - \omega_{pe}^2}{\omega^2(1 - i\frac{V_T}{V_o})^2}\right]^{-1}$$

$$= \omega_{pb}^2 \left[\frac{\omega^2 (1 - i \frac{V_T}{V_o})^2}{\omega^2 (1 - i \frac{V_T}{V_o})^2 - \omega_{pi}^2 (1 - i \frac{V_T}{V_o})^2 - \omega_{pe}} \right]$$

$$= \omega_{pb}^2 \left[\frac{\omega^2 (V^* - i\, 2 \frac{V_T}{V_o})}{\omega^* (V^* - i\, 2 \frac{V_T}{V_o}) - \omega_{pe}} \right]$$

where $V^* = 1 - (V_T/V_o)^2$, $\omega^* = \omega^2 - \omega_{pi}^2$.

Multiplying the top and bottom by the complex conjugate:

$$\delta\omega^2 = \omega_{pb}^2 \left[\frac{\omega^2 (V^* - i\, 2 \frac{V_T}{V_o})(\omega^* V^* - \omega_{pe}^2 + i\, 2 \frac{V_T}{V_o} \omega^*)}{(\omega^* V^* - \omega_{pe}^2)^2 + 4(\omega^*)^2 (\frac{V_T}{V_o})^2} \right]$$

$$= \omega_{pb}^2 [x + iy] \tag{A8}$$

$$\text{where } x = \frac{\omega^2 V^* (\omega^* V^* - \omega_{pe}^2) + 4\omega^2 (\frac{V_T}{V_o})^2 \omega^*}{(\omega^* V^* - \omega_{pe}^2)^2 + 4(\omega^*)^2 (\frac{V_T}{V_o})^2} \tag{A9}$$

$$y = \frac{2\omega^2 (\frac{V_T}{V_o}) \omega_{pe}^2}{(\omega^* V^* - \omega_{pe}^2)^2 + 4(\omega^*)^2 (\frac{V_T}{V_o})^2} \tag{A10}$$

and thus $\delta\omega$ may be found by taking the complex square root of $\omega_{pb}^2[x + iy]$

$$\delta\omega = \pm\omega_{pb}[x + iy]^{1/2}$$

or:

$$\delta\omega = \pm\sqrt{r\ e^{i\phi}}$$

where:

$$r = \sqrt{x^2 + y^2}$$

$$\phi = \tan^{-1}\left(\frac{y}{x}\right)$$ where the standard rule of quadrants is used ($\phi < 0$ if $y < 0$)

Thus:

$$\delta\omega = \sqrt{r}\ \left(\cos\frac{\phi}{2} + i\ \sin\frac{\phi}{2}\right) \qquad \text{(A11)}$$

will be the solution for the resistive-medium instability.

APPENDIX B:

PARTICLE TRAPPING COMPUTER SIMULATION

FOR A WHISTLER MODE WAVE

A simple computer study of the possibility of particle trapping in a whistler mode wave was performed. The first step in the study was to obtain the equations for the wave electric and wave magnetic fields, for a whistler mode wave propagating with a wavevector $\vec{K}$ at an angle θ to the ambient magnetic field. This was done by solving the cold plasma dispersion relation from Chapter 1 in Stix [1962] using CGS-gaussian units. From Equation 20 in Stix [1962]:

$$\begin{pmatrix} S - n^2\cos^2\theta & -iD & n^2\cos\theta\sin\theta \\ iD & S - n^2 & 0 \\ n^2\cos\theta\sin\theta & 0 & P - n^2\sin^2\theta \end{pmatrix} \begin{pmatrix} E_x \\ E_y \\ E_z \end{pmatrix} = 0 \quad \text{(B1)}$$

where the ambient magnetic field $\vec{B}_o$ is in the $\hat{Z}$ direction, the wavevector $\vec{k}$ is in the X-Z plane, and θ is the angle between $\hat{Z}$ and $\vec{k}$, where the parameters n, S, D, and P are defined in Stix [1962].

From the middle line of the matrix Equation B1:

$$iD\,E_x + (S - n^2)E_y = 0$$

which implies:

$$E_y = \frac{iD}{S - n^2}\,E_x \quad \text{(B2)}$$

From the last line of the matrix Equation B1:

$$n^2 \cos\theta \sin\theta E_x + (P - n^2\sin^2\theta)E_z = 0$$

which implies:

$$E_z = -\frac{n^2 \cos\theta \sin\theta}{P - n^2\sin^2\theta} E_x \tag{B3}$$

Assuming a wave electric field such that:

$$E_x = E_o \cos(\vec{k}\cdot\vec{r} - \omega t) \tag{B4}$$

where E_o may be complex to contain a phase constant, we can obtain by using Equations B2, B3, and B4:

$$E_y = E_o \frac{D}{S-n^2} \sin(\vec{k}\cdot\vec{r} - \omega t) \tag{B5}$$

$$E_z = E_o\left(-\frac{n^2 \cos\theta \sin\theta}{P - n^2\sin^2\theta}\right)\cos(\vec{k}\cdot\vec{r} - \omega t) \tag{B6}$$

To determine the wave magnetic field we use one of Maxwell's Equations:

$$\nabla \times \vec{E} = -\frac{1}{c}\frac{\partial \vec{B}}{\partial t}$$

and Fourier analyzing:

$$i\,\vec{k} \times \vec{E} = -\frac{1}{c}(-i\omega\vec{B})$$

or

$$\vec{k} \times \vec{E} = \frac{\omega}{c}\vec{B}$$

now defining $\vec{n} = \frac{c}{\omega}\vec{k} = (|\vec{n}|\sin\theta,\ 0,\ |\vec{n}|\cos\theta)$ where $|\vec{n}|$ is the index of refraction:

$$\vec{n} \times \vec{E} = \vec{B}$$

Thus:

$$\vec{B} = \begin{vmatrix} \hat{x} & \hat{y} & \hat{z} \\ n_x & n_y & n_z \\ E_x & E_y & E_z \end{vmatrix} \qquad \text{(B7)}$$

Solving this for the defined values of n_x, n_y and n_z:

$$B_x = -E_y\, n \cos\theta \qquad \text{(B8a)}$$

$$B_y = -E_z\, n \sin\theta + E_x\, n \cos\theta \qquad \text{(B8b)}$$

$$B_z = E_y \, n \sin \theta \qquad \text{(B8c)}$$

Thus, from a single intensity parameter of the whistler mode wave E_o, and the parameters of the wave used (ω = 1885 sec^{-1}, n_e = 1.0 cm^{-3}, and B_o = 40 gamma) all wave electric and magnetic fields can be derived from Equations B4, B5, B6, and B8.

The computer model used was to make a box with the z-axis along the $\vec{k}$ vector of the wave, where the length of the box was exactly one wavelength long. This gave periodic boundary conditions on the box where the x and y lengths were arbitrary. The electric and magnetic fields in the box were thus functions of the z-axis position and time only. The electron was injected at a velocity slightly greater than the phase velocity of the wave (corrected by $[\cos \theta]^{-1}$ term to correspond to the phase velocity along the ambient magnetic field), and the wave intensity as defined by the electric field was allowed to grow linearly with time. A fourth order Runge-Kutta solution to the first order equations for acceleration and position, using the Lorentz force equation was used. The time step was about one-twentieth of the electron gyroperiod for the results shown in Figure 16. In the cases of three different wavevector angles θ shown in Figure 16, trapping occurred when the whistler mode intensity became large enough.

APPENDIX C:

FIGURES

Figure 1 This figure shows an equatorial projection of the Earth's magnetosphere region, showing a typical ISEE orbit. It indicates by shading the general region in which the observations of the electrostatic bursts accompanied by whistler mode chorus were made. The shaded region represents only where the wideband mode utilized can observe both bursts and chorus simultaneously, and is not considered a limit on the region of occurrence. The axes have tic marks at intervals of 5 Earth radii.

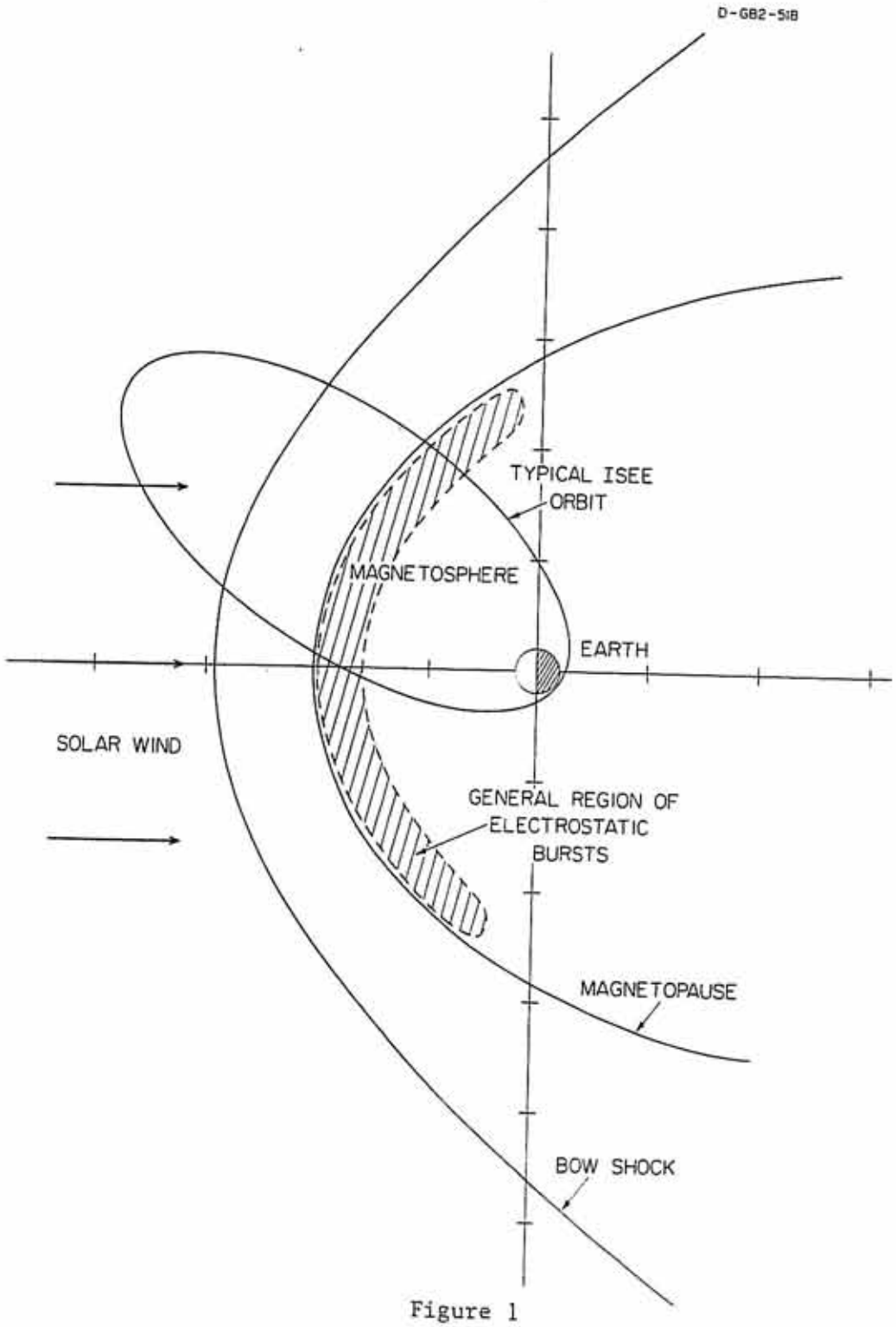
D-GB2-5IB
TYPICAL ISEE
ORBIT
MAGNETOSPHERE
EARTH
SOLAR WIND
GENERAL REGION OF
ELECTROSTATIC
BURSTS
MAGNETOPAUSE
BOW SHOCK

Figure 1

Figure 2 Diagram showing the ISEE 1 spacecraft with its various antennas. The long electric dipole antenna which has a 215 meter tip-to-tip length is the one used for all the wideband data from ISEE 1 utilized in this study. The magnetic search coil antenna and the magnetometer are shown extended on their separate booms.

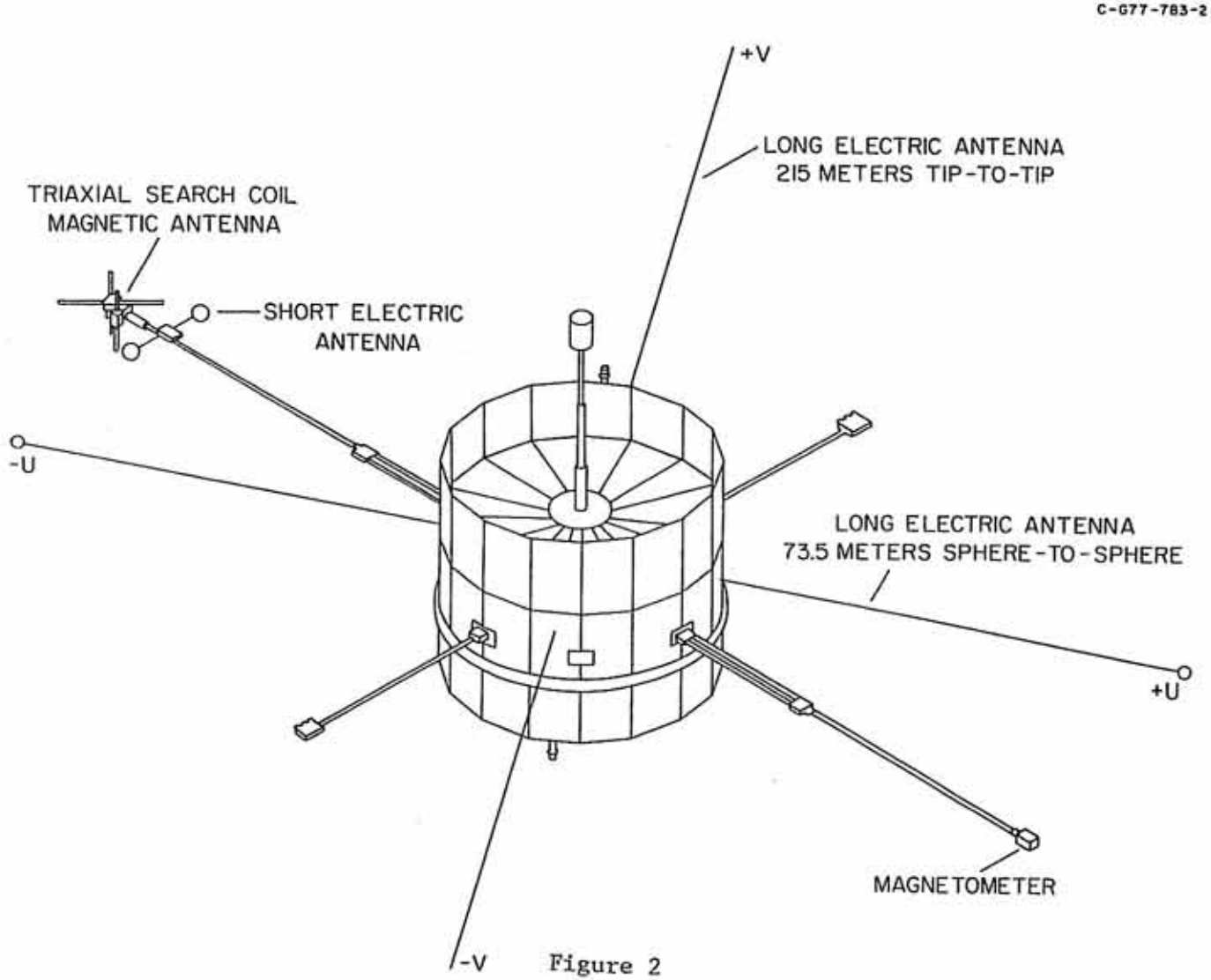
C-G77-783-2
+V
LONG ELECTRIC ANTENNA
215 METERS TIP-TO-TIP
TRIAXIAL SEARCH COIL
MAGNETIC ANTENNA
SHORT ELECTRIC
ANTENNA
-U
LONG ELECTRIC ANTENNA
73.5 METERS SPHERE-TO-SPHERE
+U
MAGNETOMETER
-V

Figure 2

Figure 3 This figure is used to show the general way in which the LEPEDEA instrument sweeps out its field of view. There are seven pairs of two detectors, totaling fourteen detectors in all. Each pair contains one detector for electrons (E) and one detector for protons (P), with identical fields of view. As the spacecraft spins through the angle ϕ, all indicated angles of θ are sampled, and 98% of the entire unit sphere is thus sampled.

LEPEDEA FIELDS-OF-VIEW
SPACECRAFT COORDINATES

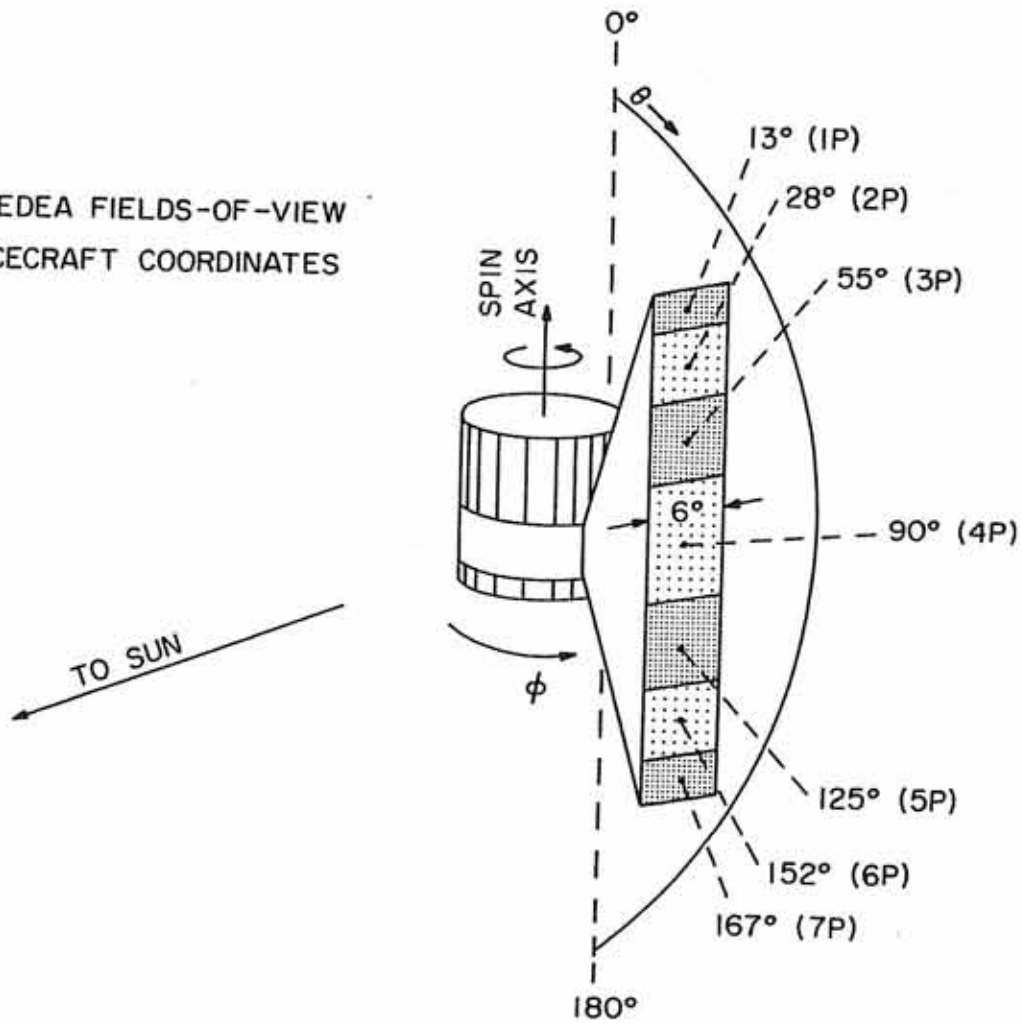

Figure 3

Figure 4 Example of one panel of a LEPEDEA E-ϕ spectrogram. The 6P at the top indicates that the data was taken by detector pair 6 (θ = 152 degrees), and the ion detector was used (P for Proton, E for Electron). Both energy and time are marked along the ordinate since 128 seconds is required in the high bit rate for an entire energy scan. The abscissa shows the solar ecliptic longitude angle of the flow direction.

A-G81-162-1

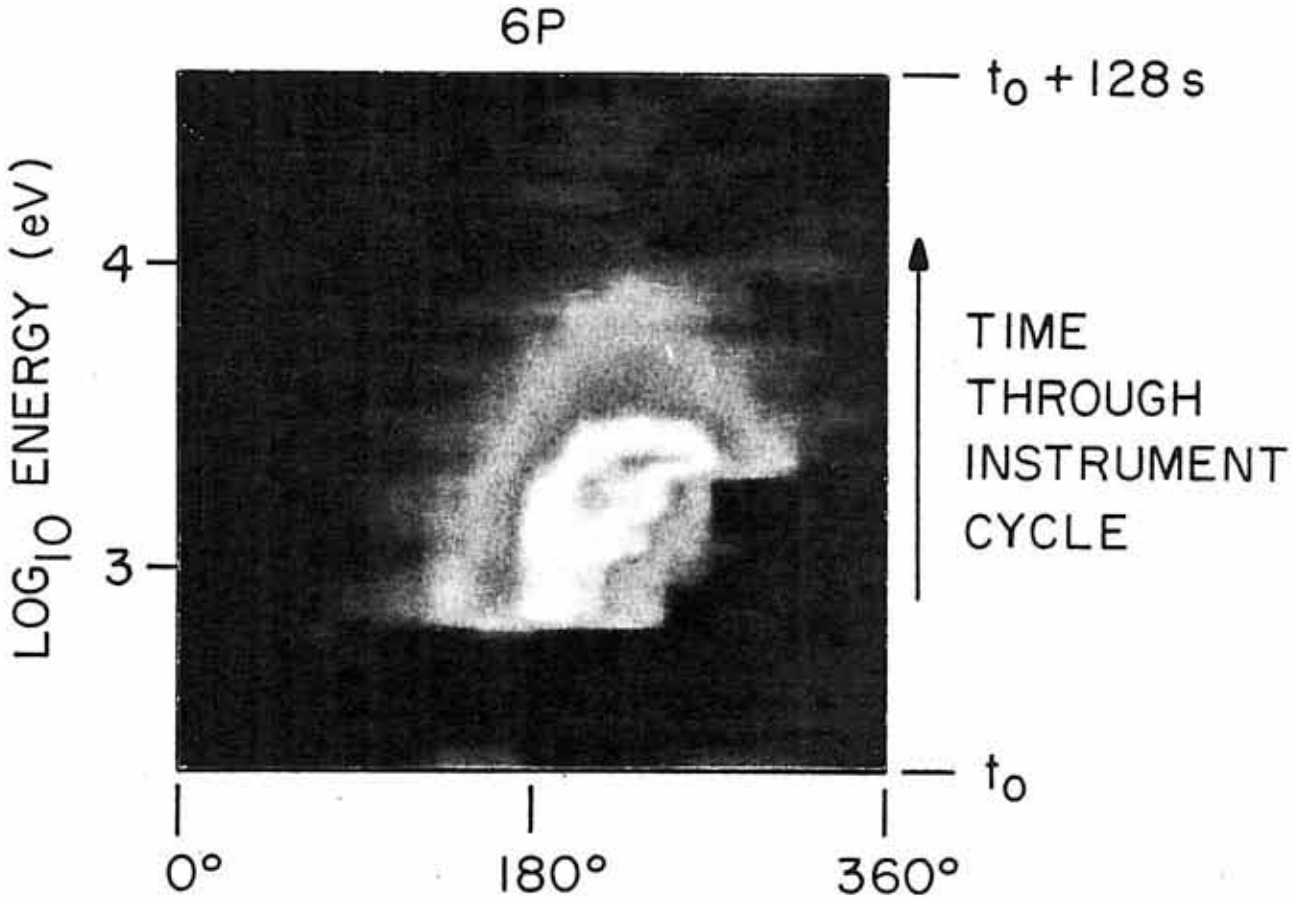

Figure 4

Figure 5 ISEE 1 frequency-time wideband data illustrating the main characteristics of the electrostatic bursts and their relationship to whistler mode chorus waves. In this case, the electrostatic bursts are correlated to the discrete chorus "hooks" in the chorus band. The bursts have a much higher frequency range than the chorus, and a wider frequency spread. The plasma frequency and the electron gyrofrequency are indicated at the right. The lower edge of the continuum radiation, indicating the plasma frequency, is much fainter in this figure than is usual. The time interval covered is three minutes.

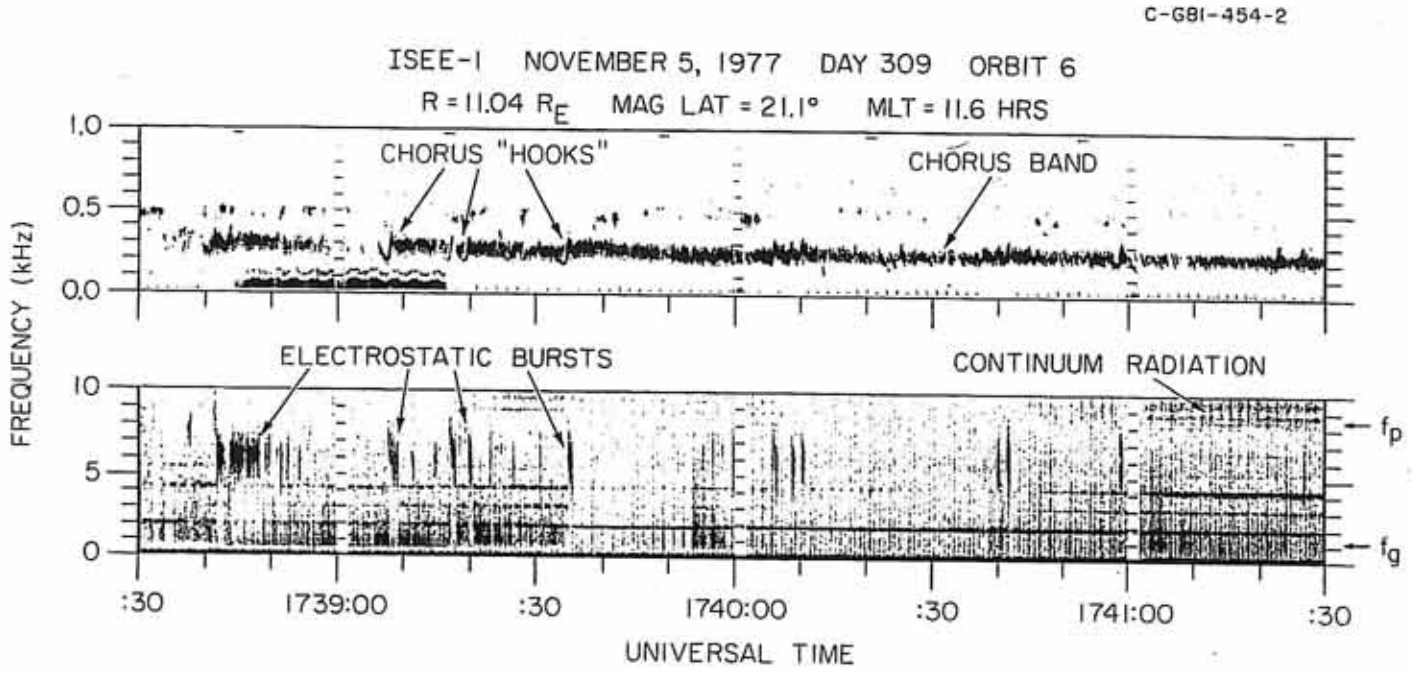
C-G81-454-2
ISEE-1 NOVEMBER 5, 1977 DAY 309 ORBIT 6
R = 11.04 R_E MAG LAT = 21.1° MLT = 11.6 HRS
CHORUS "HOOKS"
CHORUS BAND
ELECTROSTATIC BURSTS
CONTINUUM RADIATION
FREQUENCY (kHz)
1.0
0.5
0.0
10
5
0
f_p
f_g
:30
1739:00
:30
1740:00
:30
1741:00
:30
UNIVERSAL TIME

Figure 5

Figure 6 ISEE 1 frequency-time wideband data illustrating the main characteristics of the long time duration electrostatic bursts when they are correlated with an intensification of the chorus band, and no single discrete chorus feature. The time interval covered is for one minute.

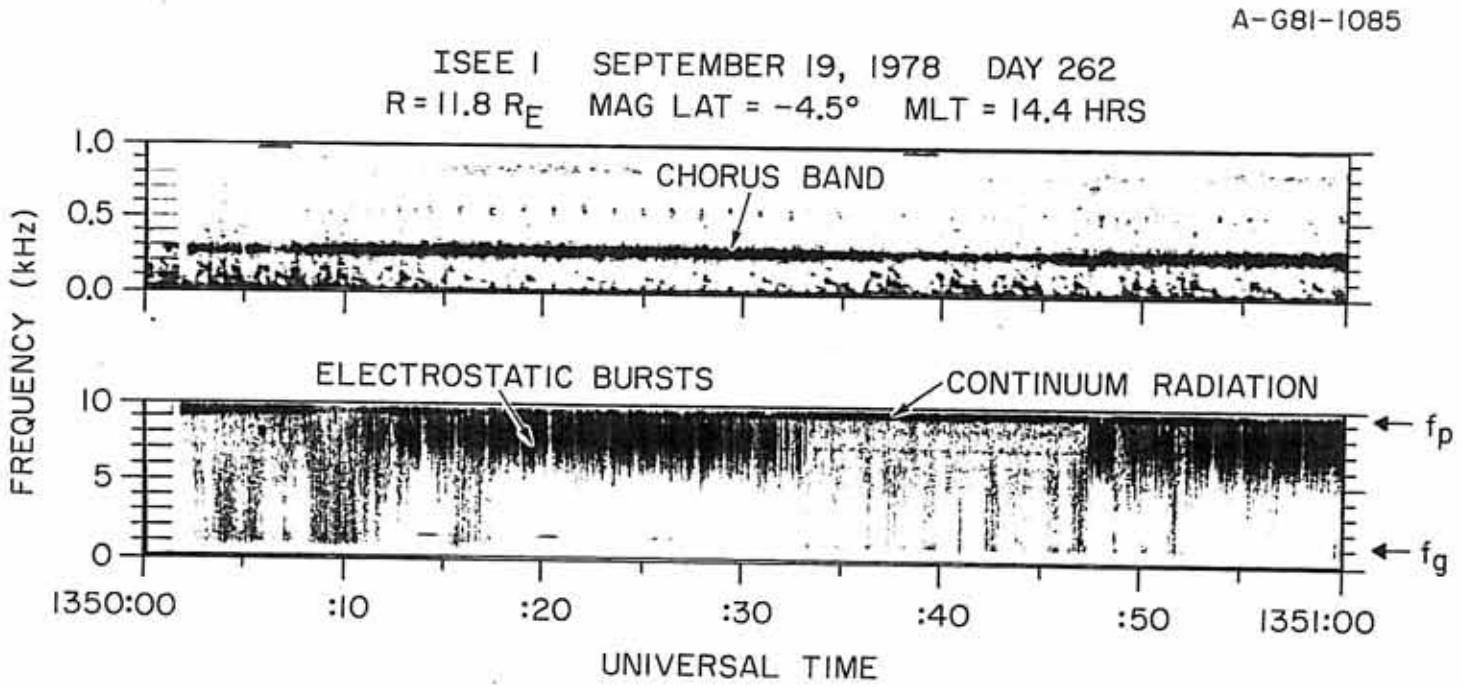
A-G81-1085
ISEE 1 SEPTEMBER 19, 1978 DAY 262
R = 11.8 R_E MAG LAT = −4.5° MLT = 14.4 HRS
CHORUS BAND
ELECTROSTATIC BURSTS
CONTINUUM RADIATION
f_p
f_g
FREQUENCY (kHz)
1.0
0.5
0.0
10
5
0
1350:00
:10
:20
:30
:40
:50
1351:00
UNIVERSAL TIME

Figure 6

Figure 7 Two sets of simultaneous frequency-time wideband data from the ISEE 1 and ISEE 2 spacecraft. The ISEE 1 wideband receiver was connected to the 215 meter long electric dipole antenna, while the ISEE 2 wideband receiver was connected to the magnetic search coil antenna. The spacecraft separation at this time is 339 km, and though some of the chorus features seem to be identical at both spacecraft, the magnetic search coil antenna on ISEE 2 has no indication of the bursts at all. This is a graphic example of the electrostatic nature of the bursts.

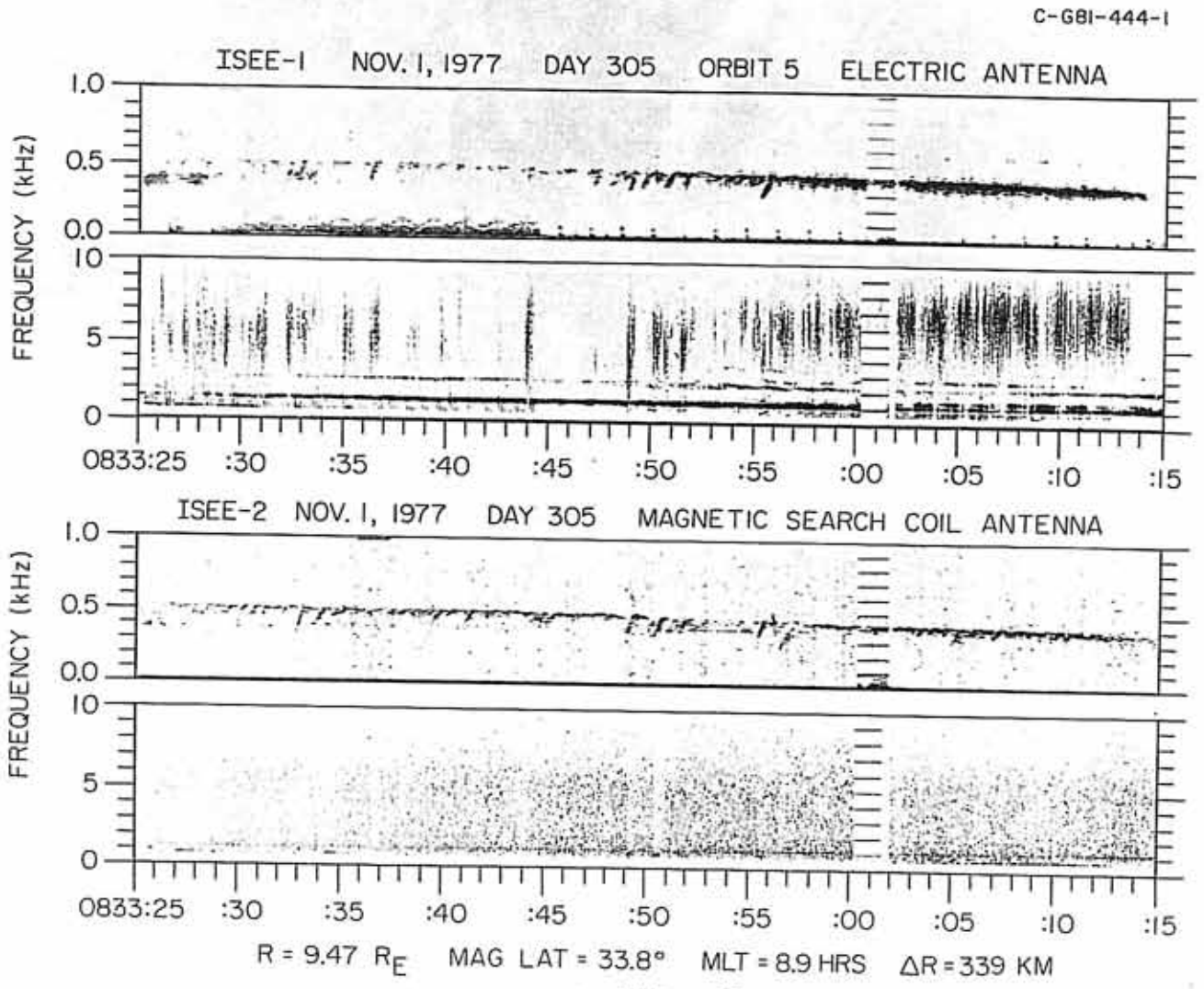
C-G81-444-1
ISEE-1 NOV. 1, 1977 DAY 305 ORBIT 5 ELECTRIC ANTENNA
FREQUENCY (kHz)
1.0
0.5
0.0
10
5
0
0833:25
:30
:35
:40
:45
:50
:55
:00
:05
:10
:15
ISEE-2 NOV. 1, 1977 DAY 305 MAGNETIC SEARCH COIL ANTENNA
FREQUENCY (kHz)
1.0
0.5
0.0
10
5
0
0833:25
:30
:35
:40
:45
:50
:55
:00
:05
:10
:15
R = 9.47 R_E MAG LAT = 33.8° MLT = 8.9 HRS ΔR = 339 KM

Figure 7

Figure 8 Frequency-time wideband data shown from the IMP 6 spacecraft, demonstrating that the electrostatic bursts correlated with chorus hooks are not features observed exclusively with the ISEE spacecraft pair. The f_p to the left indicates where the continuum radiation shows the plasma frequency. The continuum radiation can be seen faintly in the lower panel at about 0212:30 U.T., though it is clearer several minutes later, off of the figure.

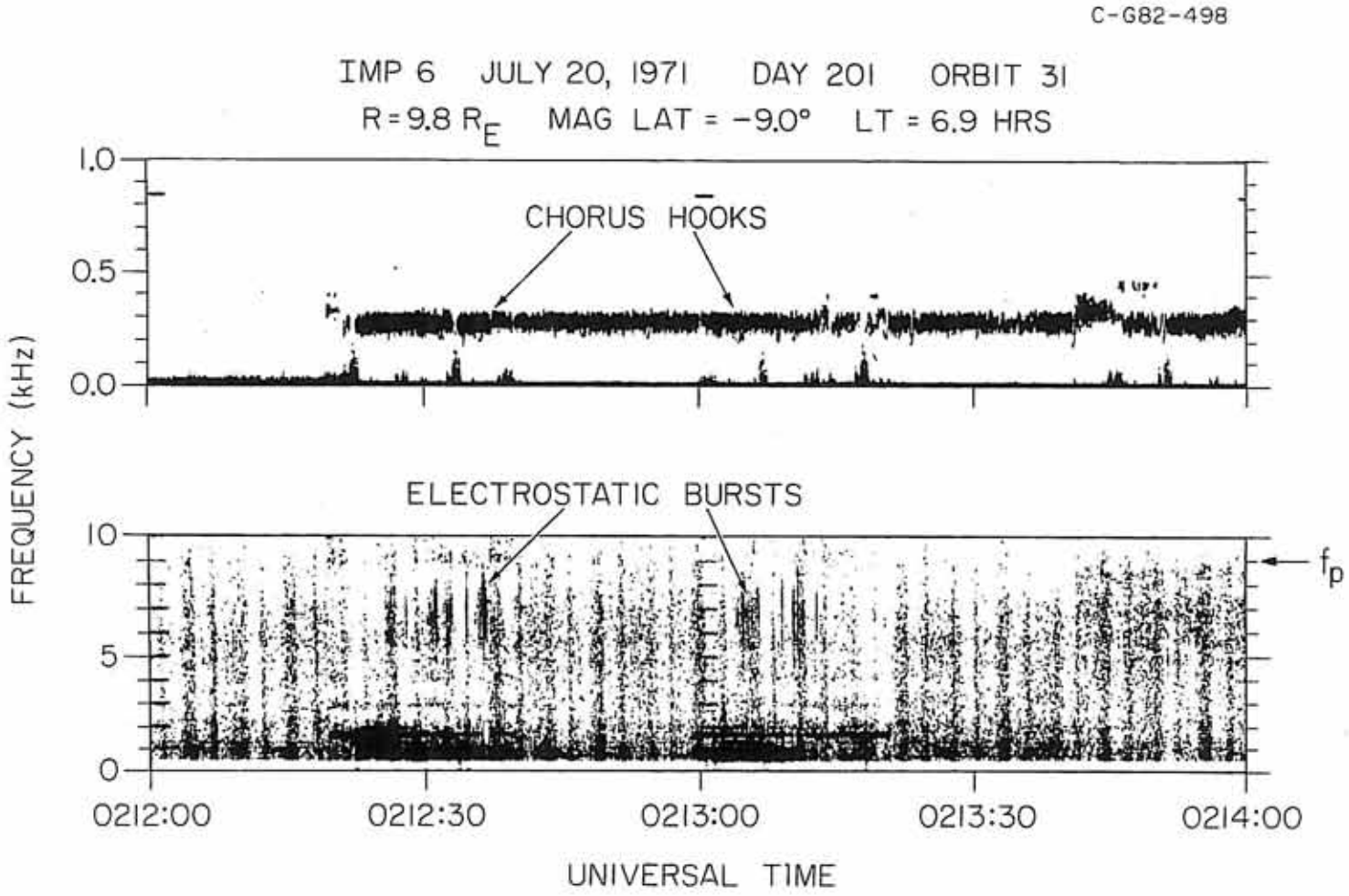
C-G82-498
IMP 6 JULY 20, 1971 DAY 201 ORBIT 31
R = 9.8 R_E MAG LAT = −9.0° LT = 6.9 HRS
1.0
0.5
0.0
CHORUS HOOKS
ELECTROSTATIC BURSTS
10
5
0
f_p
FREQUENCY (kHz)
0212:00
0212:30
0213:00
0213:30
0214:00
UNIVERSAL TIME

Figure 8

Figure 9 Another example of frequency-time wideband data taken by the IMP 6 spacecraft, showing that the longer electrostatic burst accompanying chorus band intensification is also not a feature observed exclusively with the ISEE spacecraft pair.

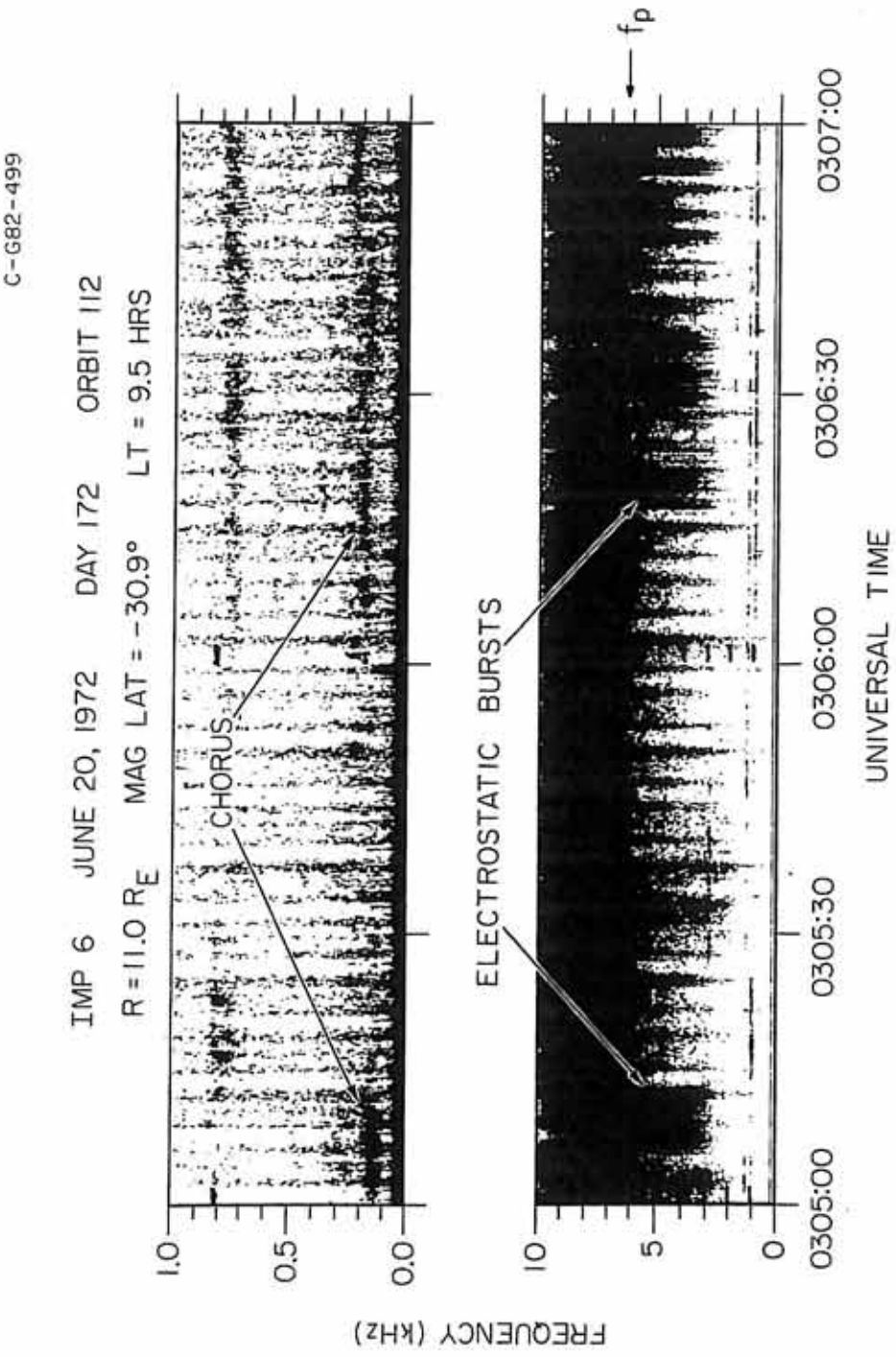
C-G82-499
IMP 6 JUNE 20, 1972 DAY 172 ORBIT 112
R = 11.0 R_E MAG LAT = -30.9° LT = 9.5 HRS
CHORUS
ELECTROSTATIC BURSTS
f_p
FREQUENCY (kHz)
1.0
0.5
0.0
10
5
0
0305:00
0305:30
0306:00
0306:30
0307:00
UNIVERSAL TIME

Figure 9

Figure 10 A blowup of a short ten-second segment of a frequency-time wideband data set, showing the occasionally observed harmonic structure of the electrostatic burst. The harmonics are not to be confused with the vertical striations due to the rapid time varying nature of the electrostatic bursts. The harmonic structure has a frequency spacing corresponding to the chorus frequency shown in the upper panel. Note that the upper panel spans only 0 to 600 Hz instead of the usual 0 to 1 kHz.

A-G81-809

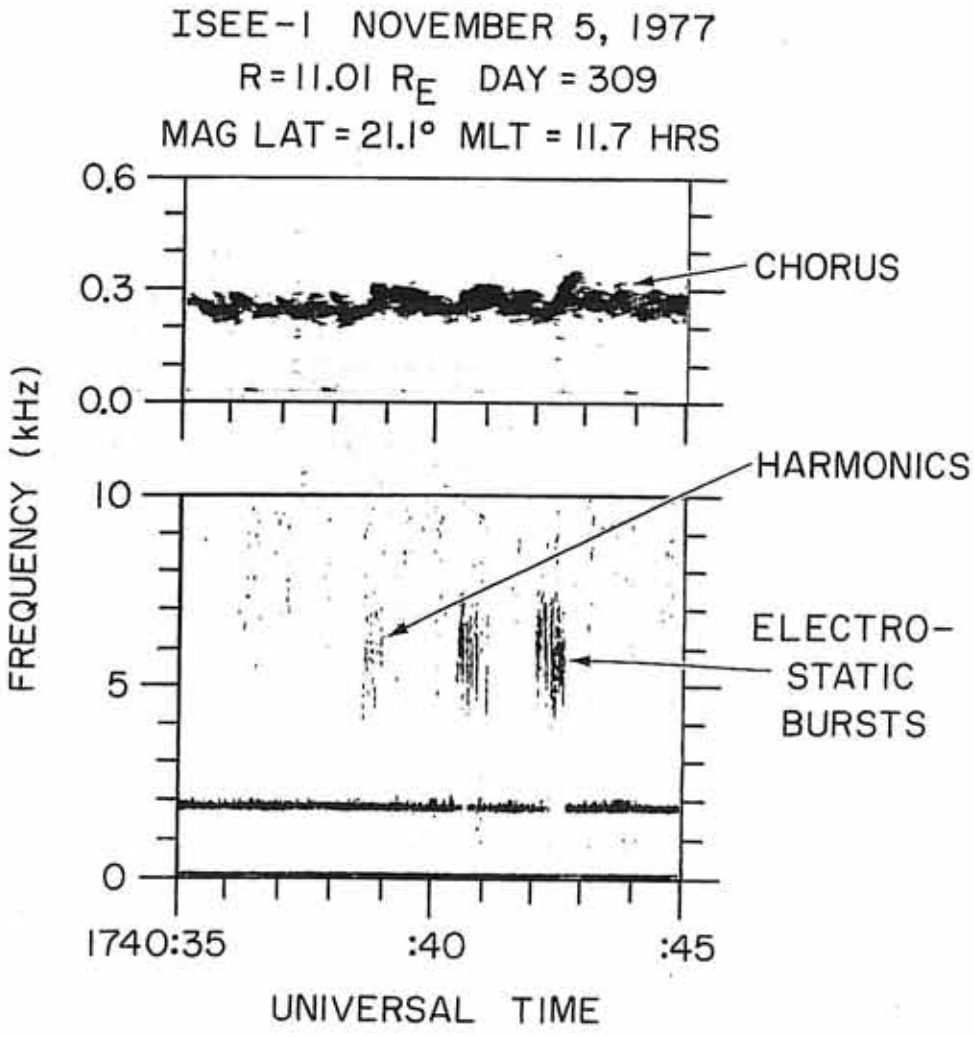

Figure 10

Figure 11 Example of the electric field spectral density versus frequency taken at both ISEE 1 and ISEE 2 during a long electrostatic burst which was observed at both spacecraft. The electric field spectral density is corrected for the different length electric dipole antennas on the two spacecraft. The fact that both the chorus and the electrostatic bursts have almost identical spectral densities indicates that the wavelengths of both waves are significantly longer than either spacecraft antenna.

A-G81-1055

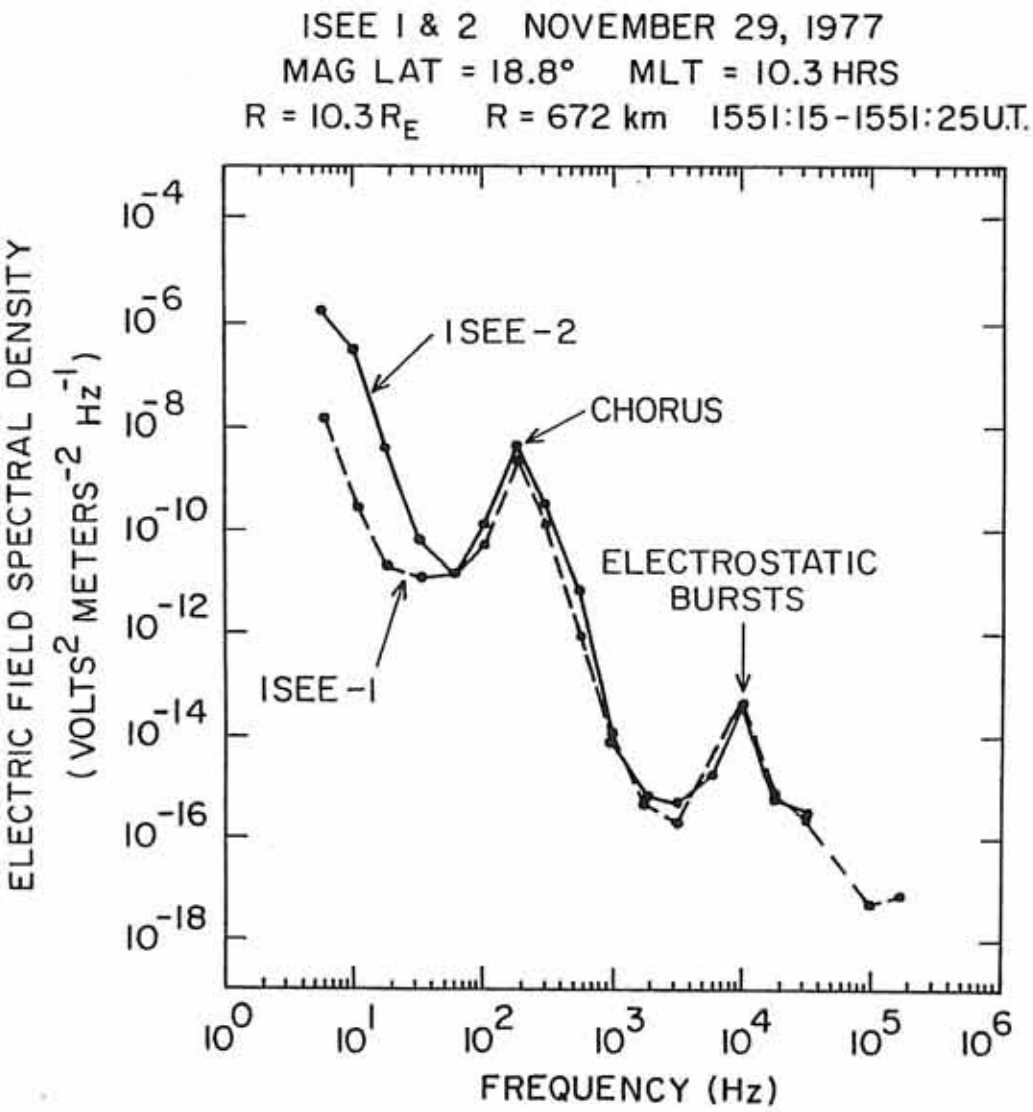

Figure 11

Figure 12 Rapid sample electric field data for the 10 kHz channel of the multichannel spectrum analyzer, showing the longitudinal nature of the electrostatic burst. The burst, centered near 10 kHz, is sampled at 32 samples per second, and is plotted against the spin angle ϕ of the spacecraft. As indicated, the maximum electric field strength is indicated when the dipole antenna was oriented along the $\vec{B}_o$ field as projected into the spin plane of the spacecraft. This indicates that the burst is longitudinally polarized with the electric field aligned approximately along the $\vec{B}_o$ field.

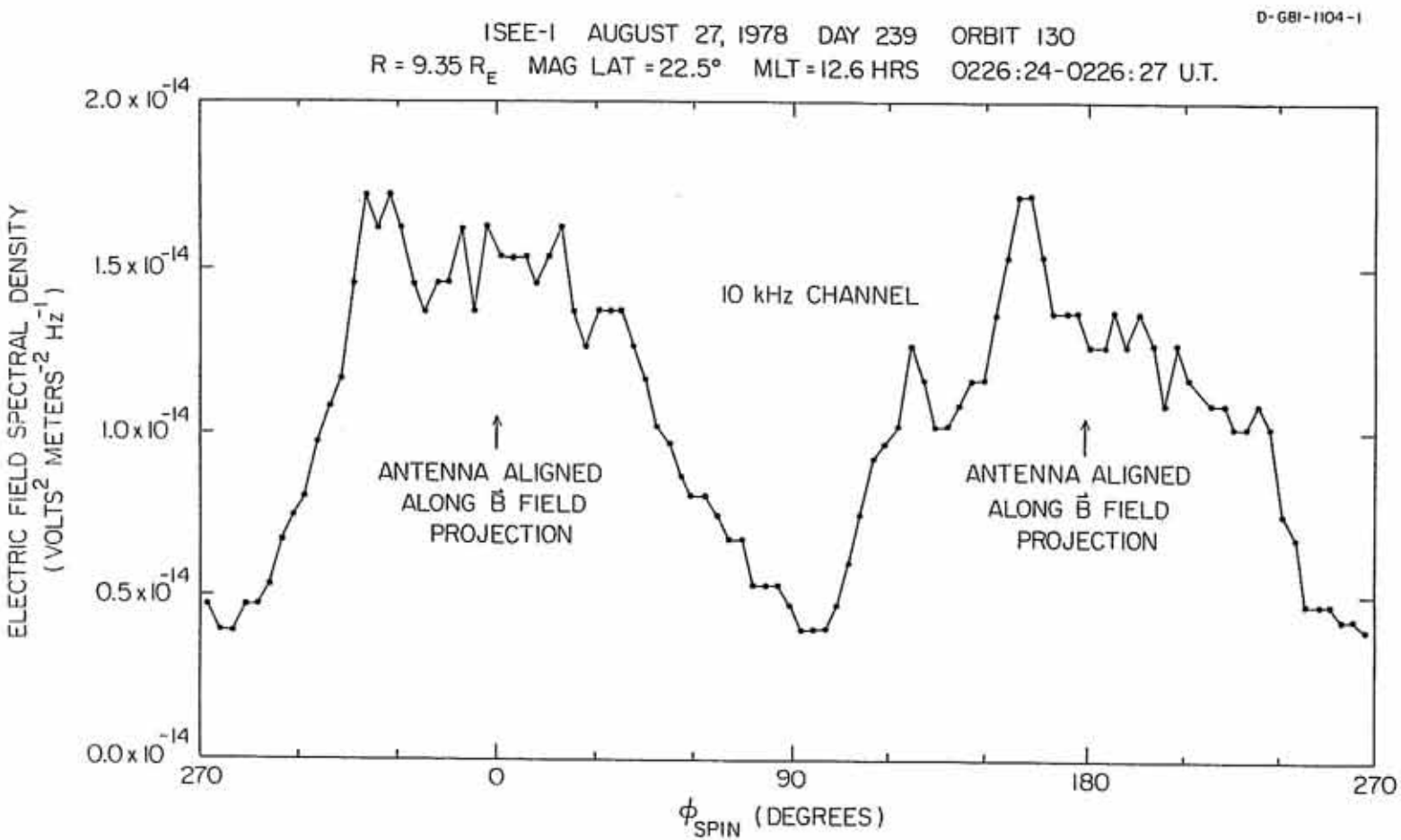
D-GBI-1104-1
ISEE-1 AUGUST 27, 1978 DAY 239 ORBIT 130
R = 9.35 R_E MAG LAT = 22.5° MLT = 12.6 HRS 0226:24-0226:27 U.T.
ELECTRIC FIELD SPECTRAL DENSITY (VOLTS^2 METERS^{-2} Hz^{-1})
2.0 x 10^{-14}
1.5 x 10^{-14}
1.0 x 10^{-14}
0.5 x 10^{-14}
0.0 x 10^{-14}
10 kHz CHANNEL
ANTENNA ALIGNED ALONG $\vec{B}$ FIELD PROJECTION
ANTENNA ALIGNED ALONG $\vec{B}$ FIELD PROJECTION
270
0
90
180
270
ϕ_{SPIN} (DEGREES)

Figure 12

Figure 13 The lower panel shows the oscilloscope waveform pattern taken from the very short burst indicated in the upper panels of frequency-time wideband data of the ISEE 1 spacecraft. The low frequency signal in the bottom of the lower panel is the chorus waveform, while the high frequency signal bursts at the top of the lower panel are the electrostatic bursts. The phase of the chorus waveform may differ from that shown by a constant phase factor. It should be noted that the lower panel is only eight milliseconds in duration.

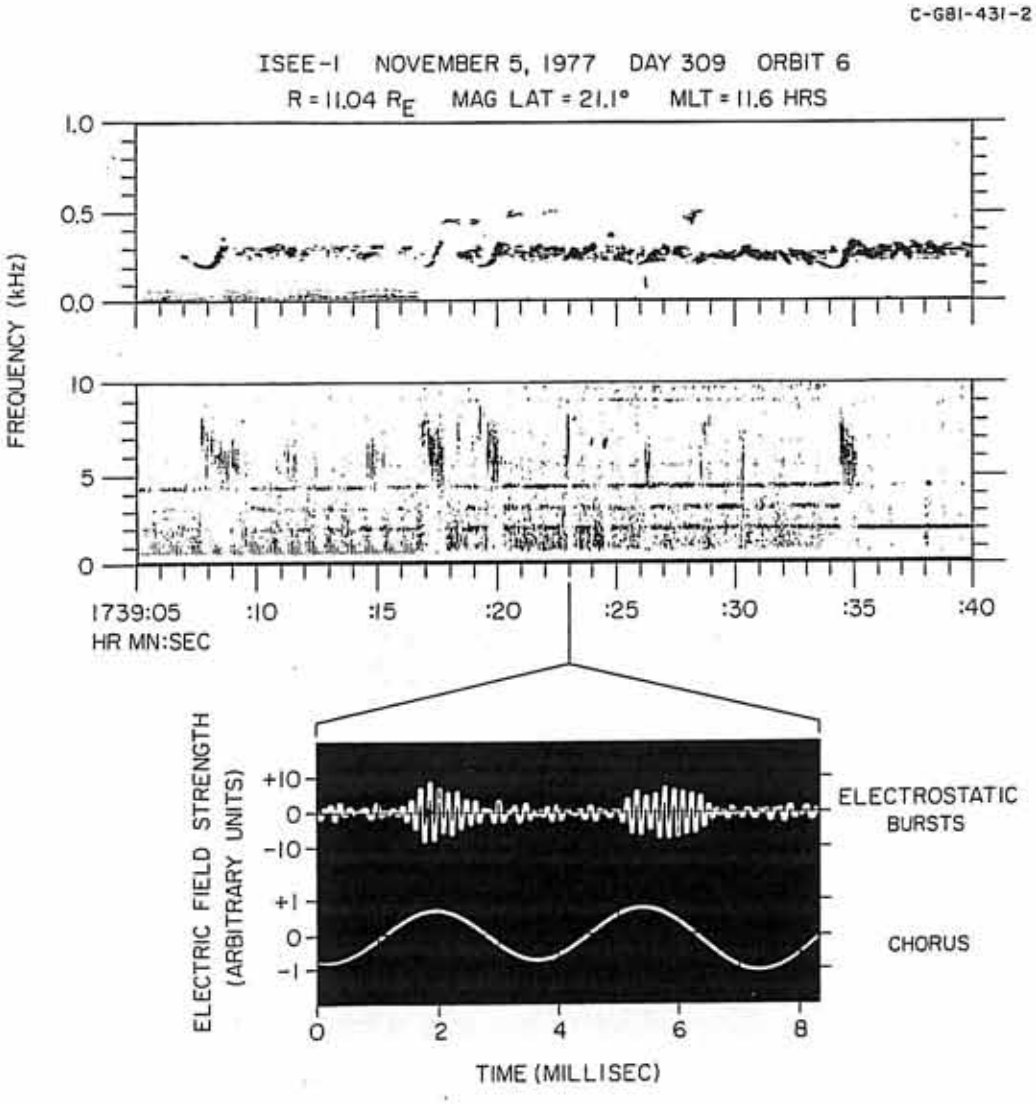
C-G81-431-2
ISEE-1 NOVEMBER 5, 1977 DAY 309 ORBIT 6
R = 11.04 R_E MAG LAT = 21.1° MLT = 11.6 HRS
FREQUENCY (kHz)
1.0
0.5
0.0
10
5
0
1739:05
HR MN:SEC
:10
:15
:20
:25
:30
:35
:40
ELECTRIC FIELD STRENGTH
(ARBITRARY UNITS)
+10
0
-10
+1
0
-1
ELECTROSTATIC
BURSTS
CHORUS
0
2
4
6
8
TIME (MILLISEC)

Figure 13

Figure 14 Four examples of oscilloscope waveform patterns are shown. In all cases the top trace is that of the chorus while the bottom trace is that of the electrostatic burst. The two left examples (A and B) are taken from a short burst correlated with a chorus hook, and have different time scales, (B) being an expansion of part of (A). The modulation effect on the bursts is very evident. The two right examples (C and D) are from a long burst just a few minutes earlier. These again have different time scales, (D) being an expansion of (C). The modulation effect on the bursts is much diminished in this case.

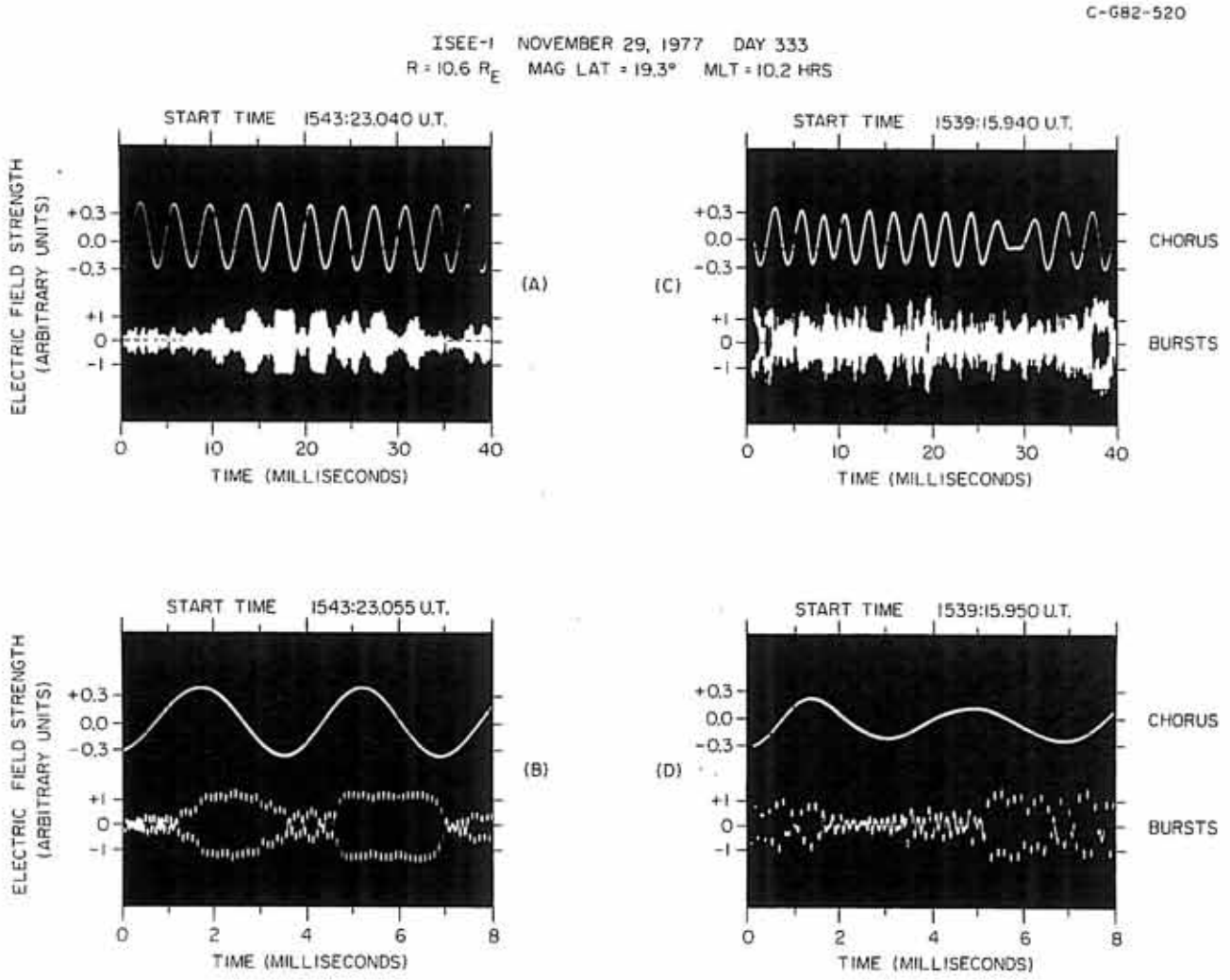
C-G82-520
ISEE-1 NOVEMBER 29, 1977 DAY 333
R = 10.6 R_E MAG LAT = 19.3° MLT = 10.2 HRS
START TIME 1543:23.040 U.T.
ELECTRIC FIELD STRENGTH (ARBITRARY UNITS)
+0.3
0.0
-0.3
+1
0
-1
0 10 20 30 40
TIME (MILLISECONDS)
(A)
START TIME 1539:15.940 U.T.
(C)
CHORUS
BURSTS
START TIME 1543:23.055 U.T.
0 2 4 6 8
(B)
START TIME 1539:15.950 U.T.
(D)

Figure 14

Figure 15 Four examples of oscilloscope waveform patterns for two different days are shown. The two right examples (A and B) are from a long burst, and do not show a strong modulation effect on the bursts. The two left examples (C and D) are from a long burst that had an odd characteristic of almost no frequency spread, and of being almost exactly at the plasma frequency as defined by the continuum radiation. No modulation of the burst is seen at all.

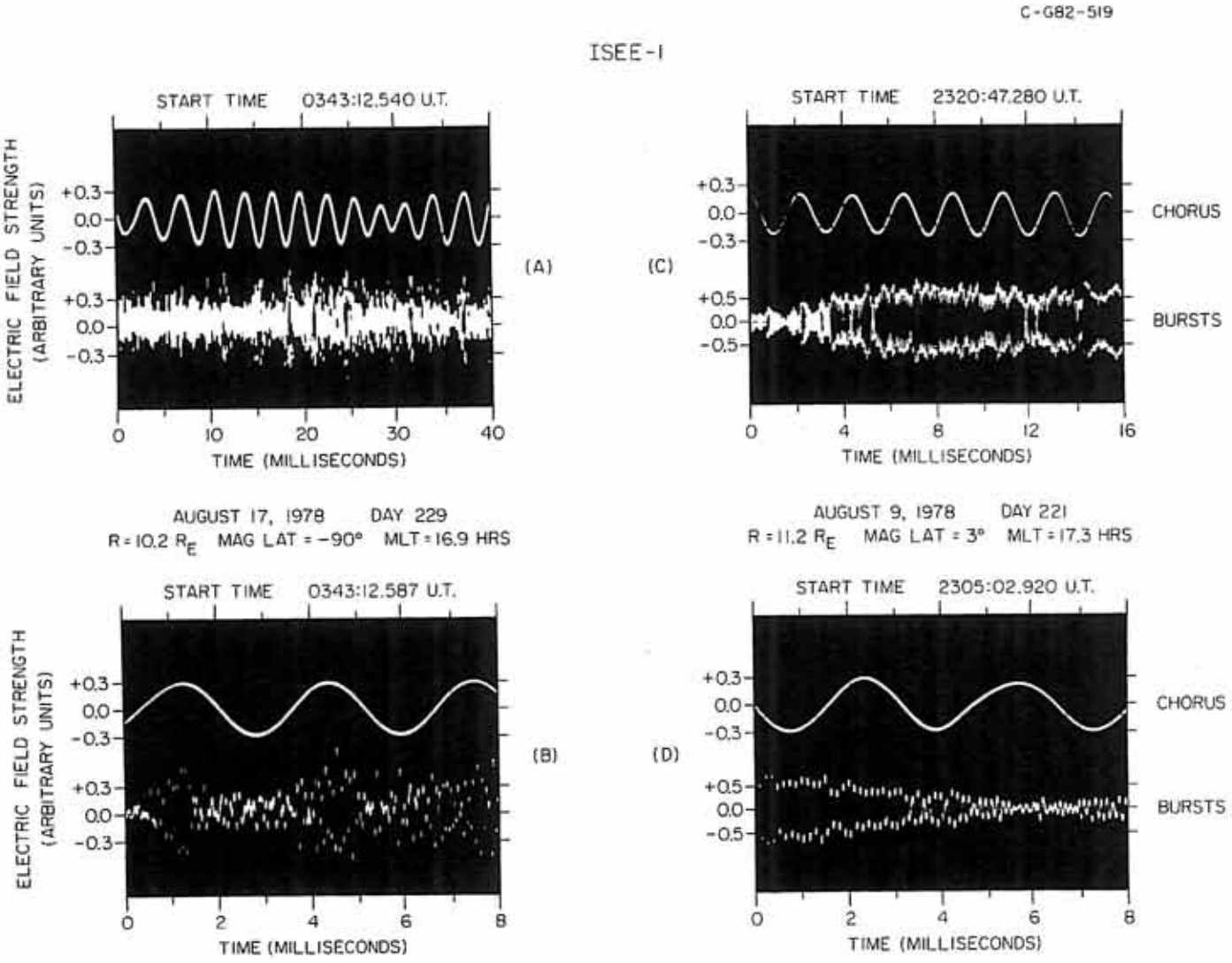
C-G82-519
ISEE-1
START TIME 0343:12.540 U.T.
ELECTRIC FIELD STRENGTH (ARBITRARY UNITS)
+0.3
0.0
-0.3
+0.3
0.0
-0.3
(A)
0
10
20
30
40
TIME (MILLISECONDS)
START TIME 2320:47.280 U.T.
+0.3
0.0
-0.3
CHORUS
+0.5
0.0
-0.5
BURSTS
(C)
0
4
8
12
16
TIME (MILLISECONDS)
AUGUST 17, 1978 DAY 229
R = 10.2 R_E MAG LAT = -90° MLT = 16.9 HRS
AUGUST 9, 1978 DAY 221
R = 11.2 R_E MAG LAT = 3° MLT = 17.3 HRS
START TIME 0343:12.587 U.T.
ELECTRIC FIELD STRENGTH (ARBITRARY UNITS)
+0.3
0.0
-0.3
+0.3
0.0
-0.3
(B)
0
2
4
6
8
TIME (MILLISECONDS)
START TIME 2305:02.920 U.T.
+0.3
0.0
-0.3
CHORUS
+0.5
0.0
-0.5
BURSTS
(D)
0
2
4
6
8
TIME (MILLISECONDS)

Figure 15

Figure 16 Illustration of the model proposed for whistler mode electron trapping and burst generation. The top panel shows how the wavevector angle will produce an $\vec{E}_{\parallel}$(parallel), while the middle panel illustrates how an electron confined to the $\vec{B}_o$ field line will see an effective potential and can be trapped at the whistler mode phase velocity. The lower panel shows how these trapped and spatially bunched electrons will generate electrostatic bursts modulated at the chorus phase velocity.

B-G81-1096

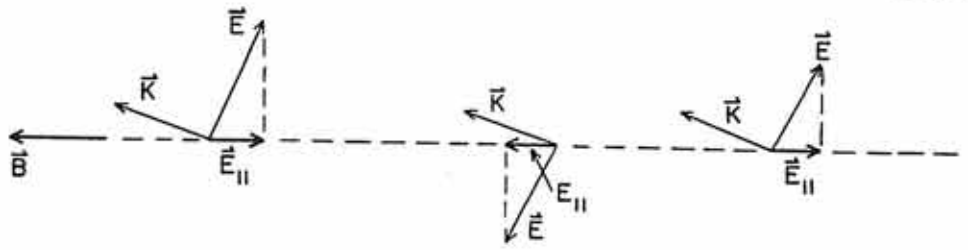

CHORUS WAVE COMPONENTS

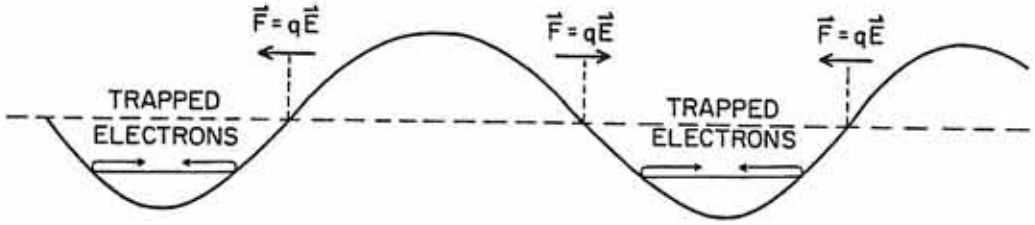

EFFECTIVE POTENTIAL

ELECTROSTATIC BURSTS

Figure 16

Figure 17 Three cases of particle trapping produced by computer modeling for different wave vector angles (θ) to the ambient $\vec{B}_o$ field. Z-phase is the phase relation between the electron and the whistler mode wave. Trapping is defined when the phase variation is bounded. In the model, the electric field intensity of the whistler mode wave increased linearly with time, and so the abscissa is marked as both time and E_o.

C-GB2-523-1

PARTICLE TRAPPING FROM COMPUTER MODEL

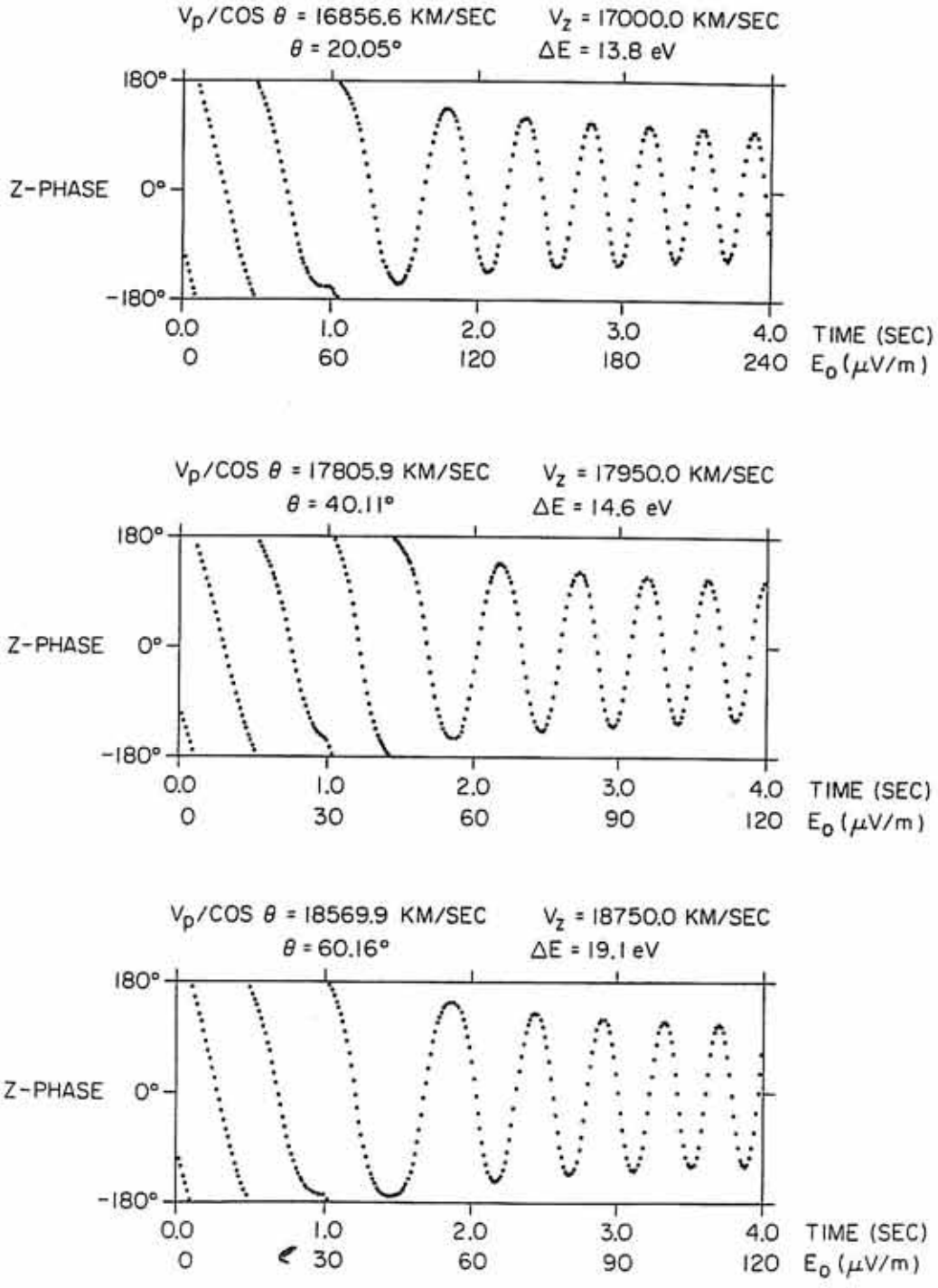

Figure 17

Figure 18 Illustration of a suggested possibility for production of a distinct electron beam in the distribution function. In this suggested scenerio, the chorus wave phase velocity increases and trapped electrons are accelerated. The velocity increase has been exaggerated.

A-G81-1097

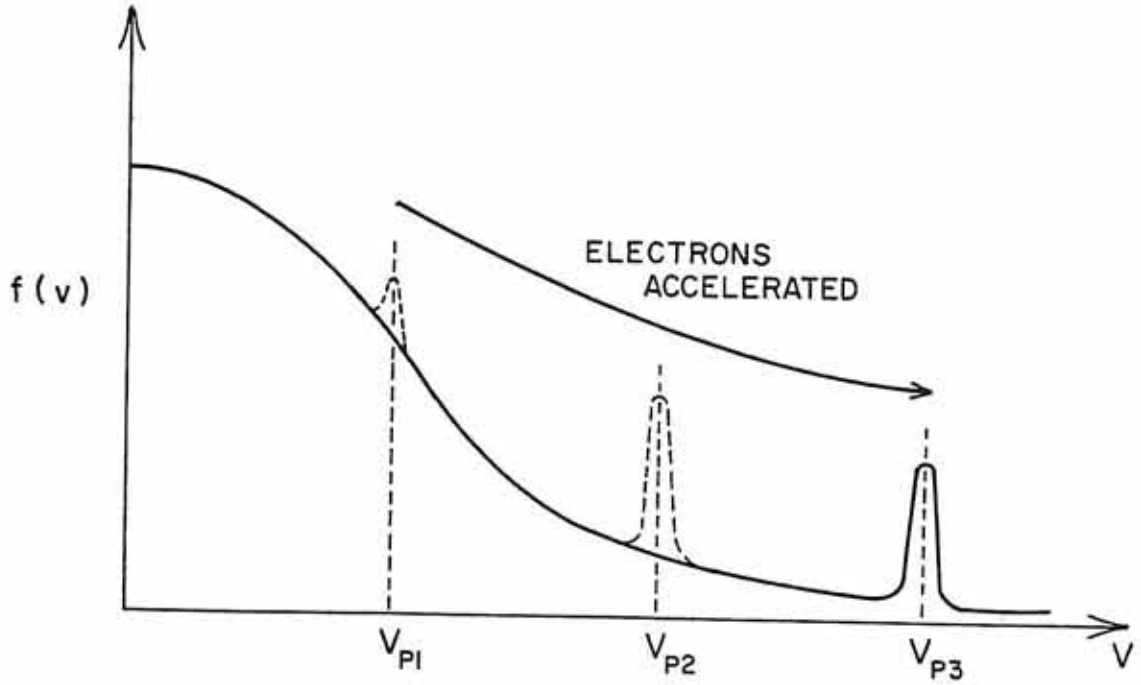

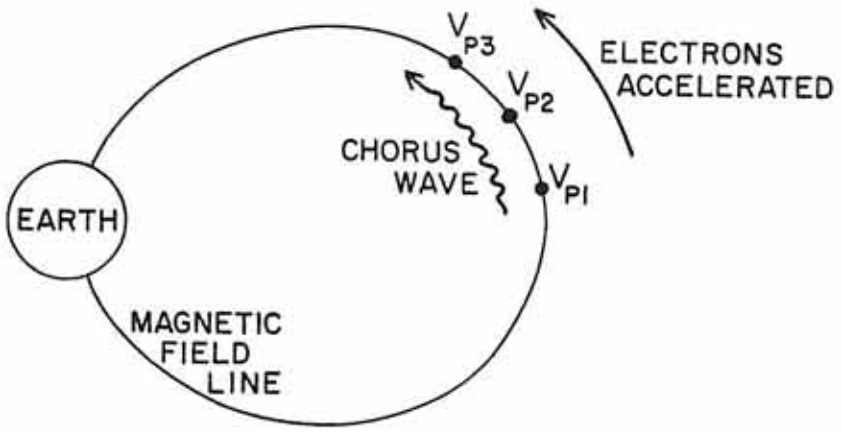

V_{PHASE} INCREASE $\Longrightarrow$ ACCELERATION OF TRAPPED ELECTRONS

Figure 18

Figure 19 E-ϕ spectrogram for day 222 in 1979 from the LEPEDEA data on the ISEE 1 spacecraft. The features pointed to by the arrows are the ambient magnetic field-aligned electron distribution function enhancements, which occured simultaneously with the long electrostatic burst.

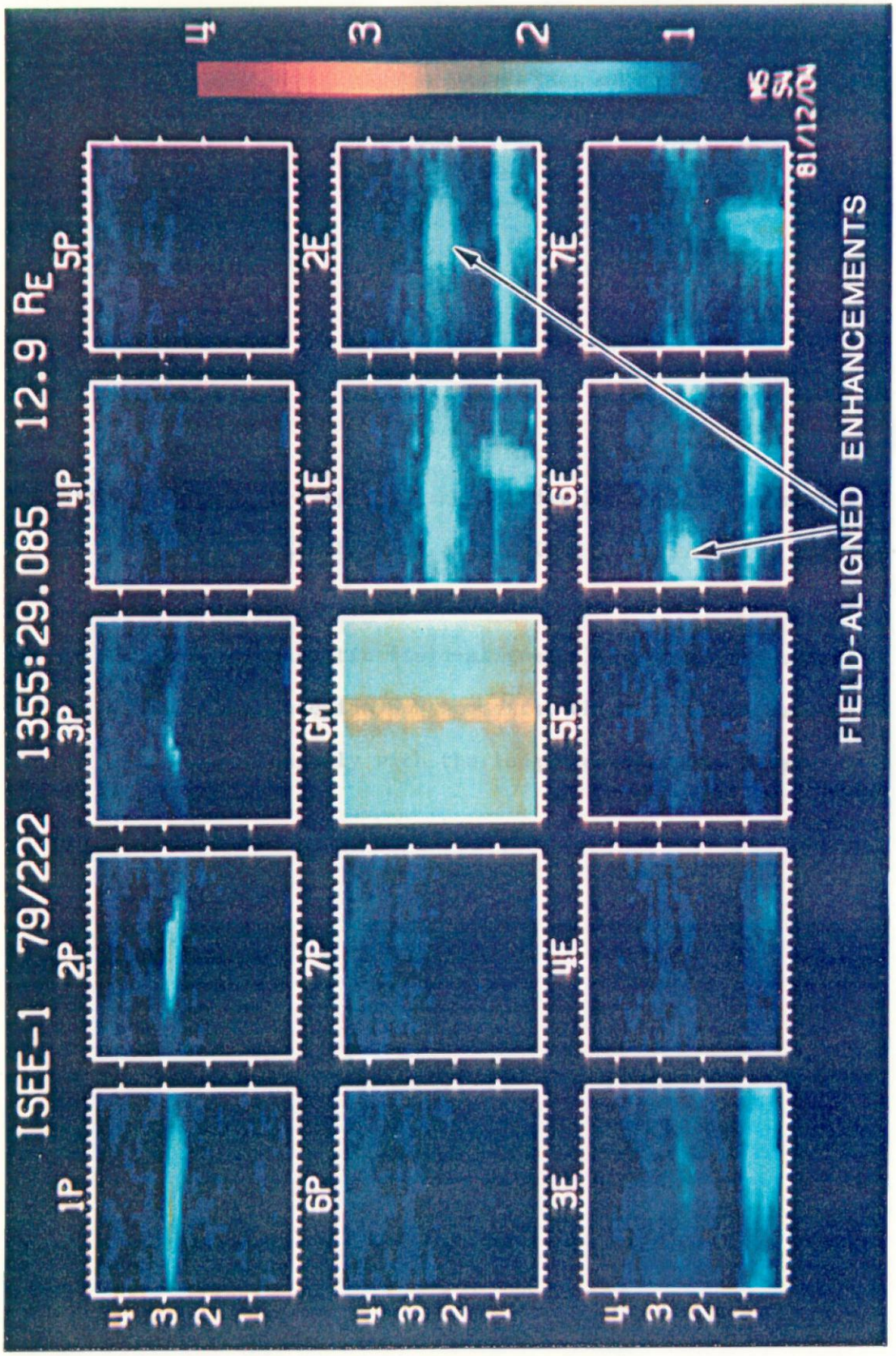
ISEE-1 79/222 1355:29.085 12.9 RE
1P
2P
3P
4P
5P
6P
7P
GM
1E
2E
3E
4E
5E
6E
7E
4
3
2
1
81/12/04
FIELD-ALIGNED ENHANCEMENTS

Figure 19

Figure 20 E-ϕ spectrogram for day 263 in 1980 from the LEPEDEA data on the ISEE 1 spacecraft. The features pointed to by the arrows are the ambient magnetic field-aligned electron distribution function enhancements, which occured simultaneously with the long electrostatic burst.

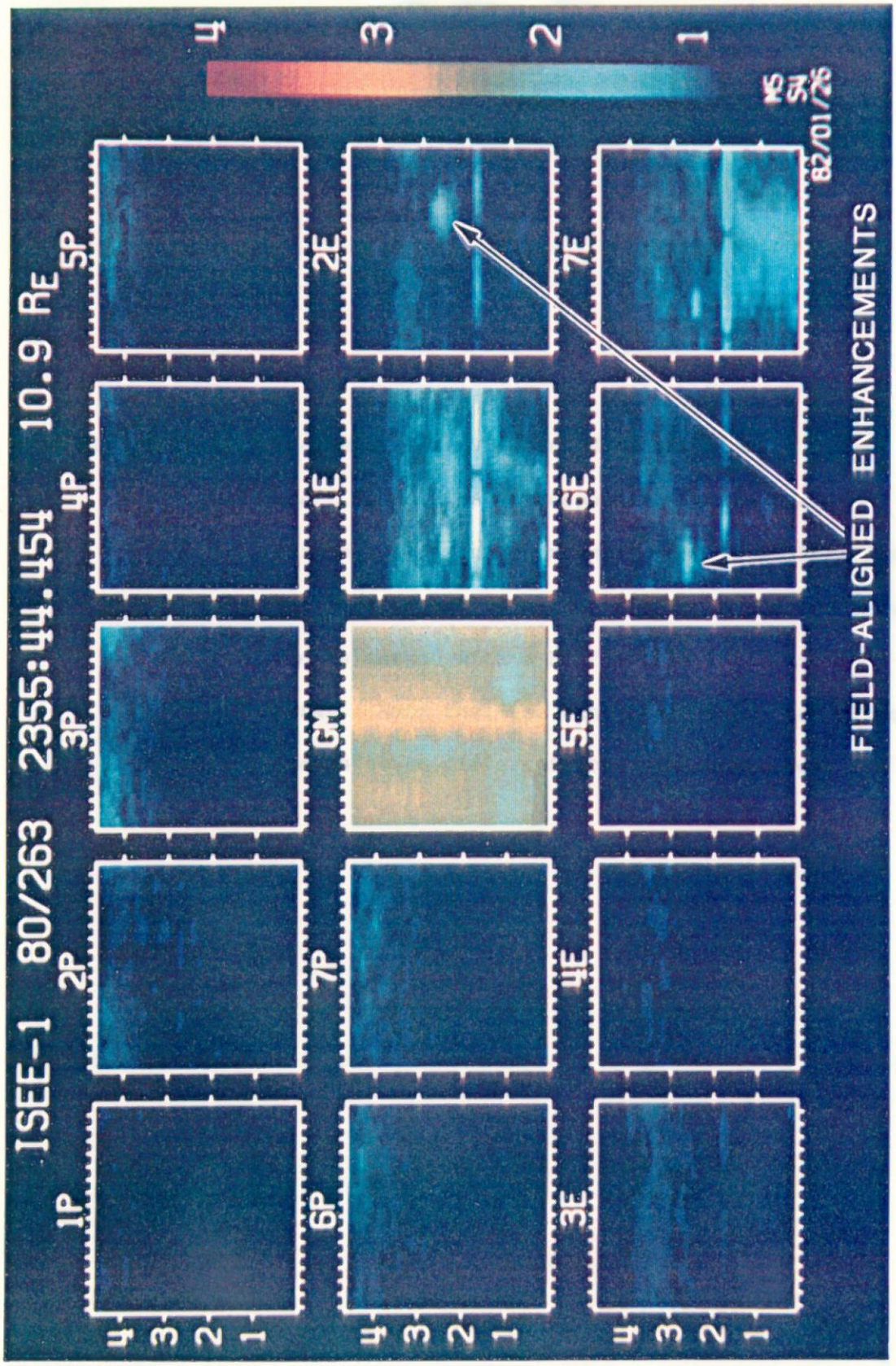
ISEE-1 80/263 2355:44.454 10.9 RE
1P
2P
3P
4P
5P
6P
7P
GM
1E
2E
3E
4E
5E
6E
7E
4 3 2 1
FIELD-ALIGNED ENHANCEMENTS

Figure 20

Figure 21 Frequency-time wideband data from ISEE 1 spacecraft for a time corresponding to the field-aligned electron enhancement seen in LEPEDEA data. The burst start is marked with an A and the burst end is marked with a B, for this 2 1/2 minute burst. Note that the time scale shows ten minutes and is quite different from previous cases.

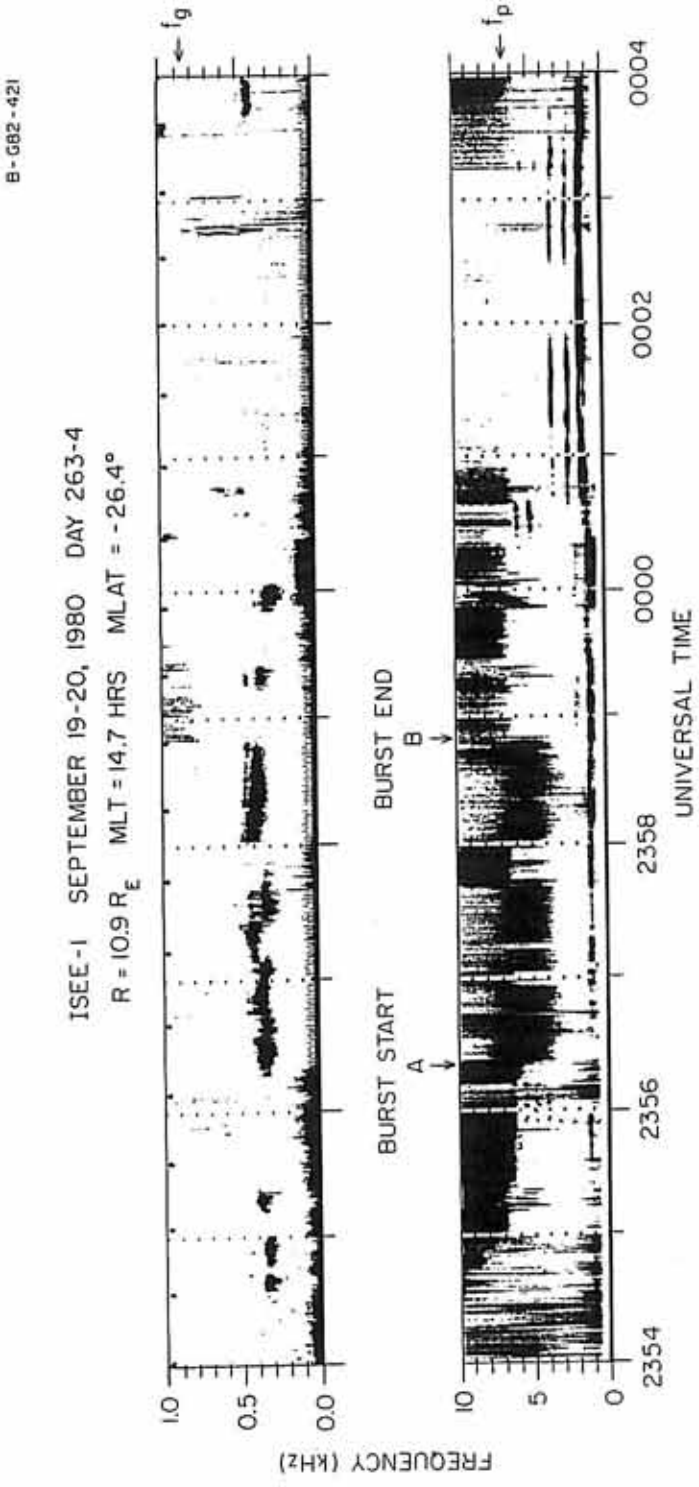
B-G82-421
ISEE-1 SEPTEMBER 19-20, 1980 DAY 263-4
R = 10.9 R_E MLT = 14.7 HRS MLAT = -26.4°
f_g
f_p
BURST START
A
BURST END
B
FREQUENCY (kHz)
1.0
0.5
0.0
10
5
0
2354
2356
2358
0000
0002
0004
UNIVERSAL TIME

Figure 21

Figure 22 Time mosaic of detectors 2E and 6E from the E-ϕ spectrograms for approximately the ten-minute interval corresponding to the wideband data in Figure 21. The A and B marks the burst start and end times respectively for the electrostatic burst shown in Figure 21. It is clear that the field-aligned enhancement at ≈ 400 eV is strongest during the burst period, but also persists slightly for several minutes after the burst end.

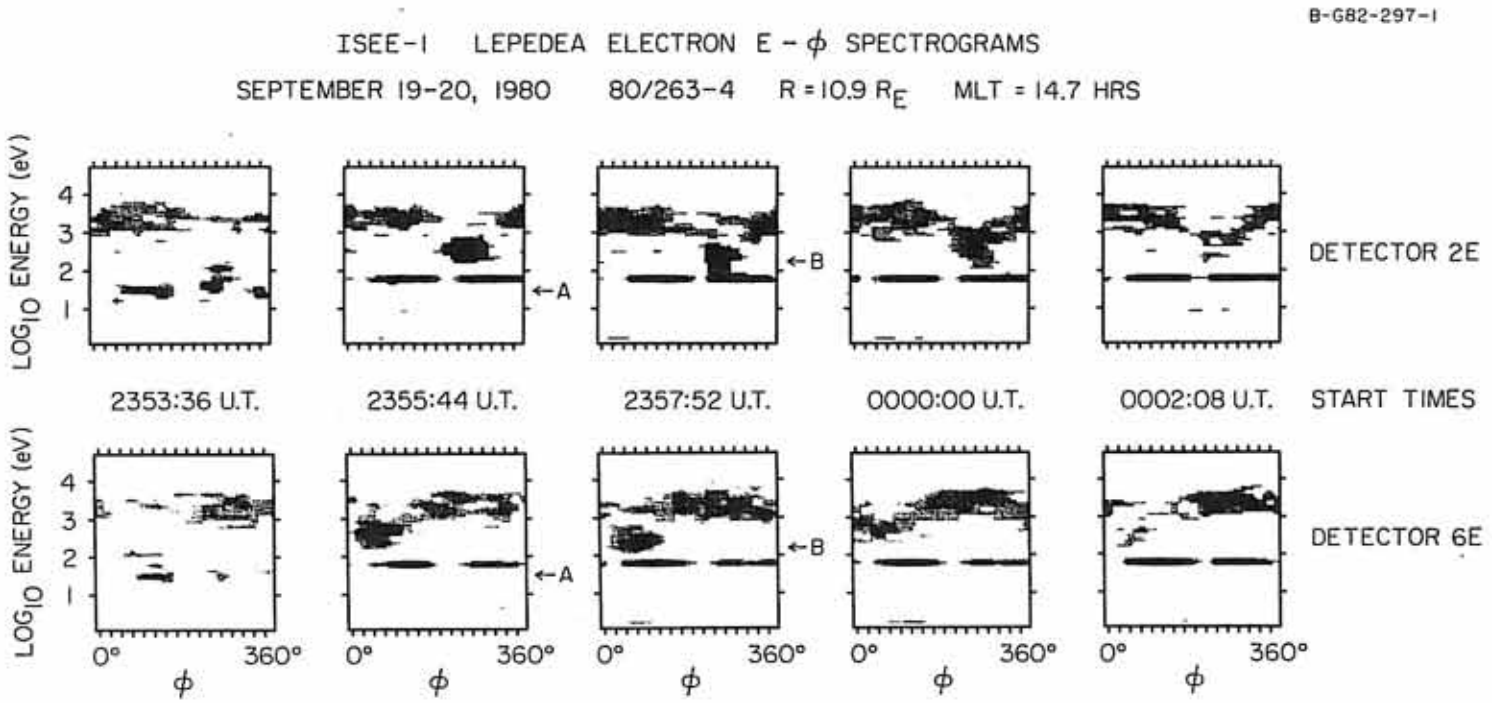
B-G82-297-1
ISEE-1 LEPEDEA ELECTRON E - φ SPECTROGRAMS
SEPTEMBER 19-20, 1980 80/263-4 R = 10.9 R_E MLT = 14.7 HRS
LOG_{10} ENERGY (eV)
4
3
2
1
←A
←B
DETECTOR 2E
2353:36 U.T.
2355:44 U.T.
2357:52 U.T.
0000:00 U.T.
0002:08 U.T.
START TIMES
DETECTOR 6E
0°
360°
φ

Figure 22

Figure 23 Perspective plot from LEPEDEA data for day 222/79 showing the electron distribution function. The two counterstreaming magnetic field-aligned electron enhancements are indicated.

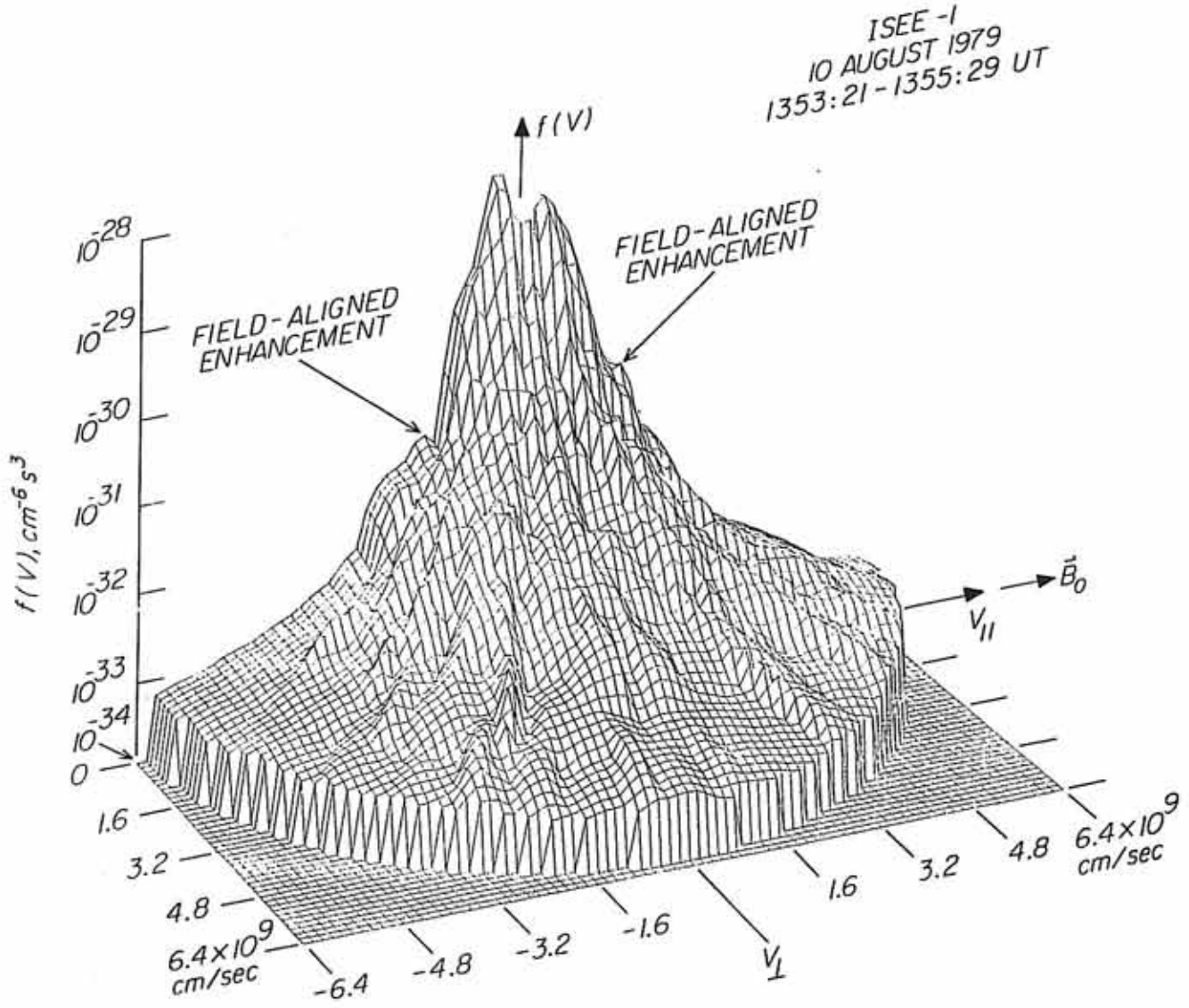
ISEE -1
10 AUGUST 1979
1353:21 - 1355:29 UT
f(V)
FIELD-ALIGNED ENHANCEMENT
FIELD-ALIGNED ENHANCEMENT
f(V), cm⁻⁶ s³
10⁻²⁸
10⁻²⁹
10⁻³⁰
10⁻³¹
10⁻³²
10⁻³³
10⁻³⁴
0
B₀
V₁₁
1.6
3.2
4.8
6.4×10⁹ cm/sec
-6.4
-4.8
-3.2
-1.6
V⊥
1.6
3.2
4.8
6.4×10⁹ cm/sec

Figure 23

Figure 24 Graph of the imaginary component of ω versus the real component of ω for the resistive-medium instability with several different values of V_o/V_T. The downshift in frequency of the maximum growth rate below the plasma frequency (ω_{pe}) for progressively lower values of V_o/V_T is very clear. The dotted lines are used to calculate the theory points in Figure 26.

A-G82-506

Im (ω) VERSUS Re (ω) FOR THE
RESISTIVE-MEDIUM INSTABILITY

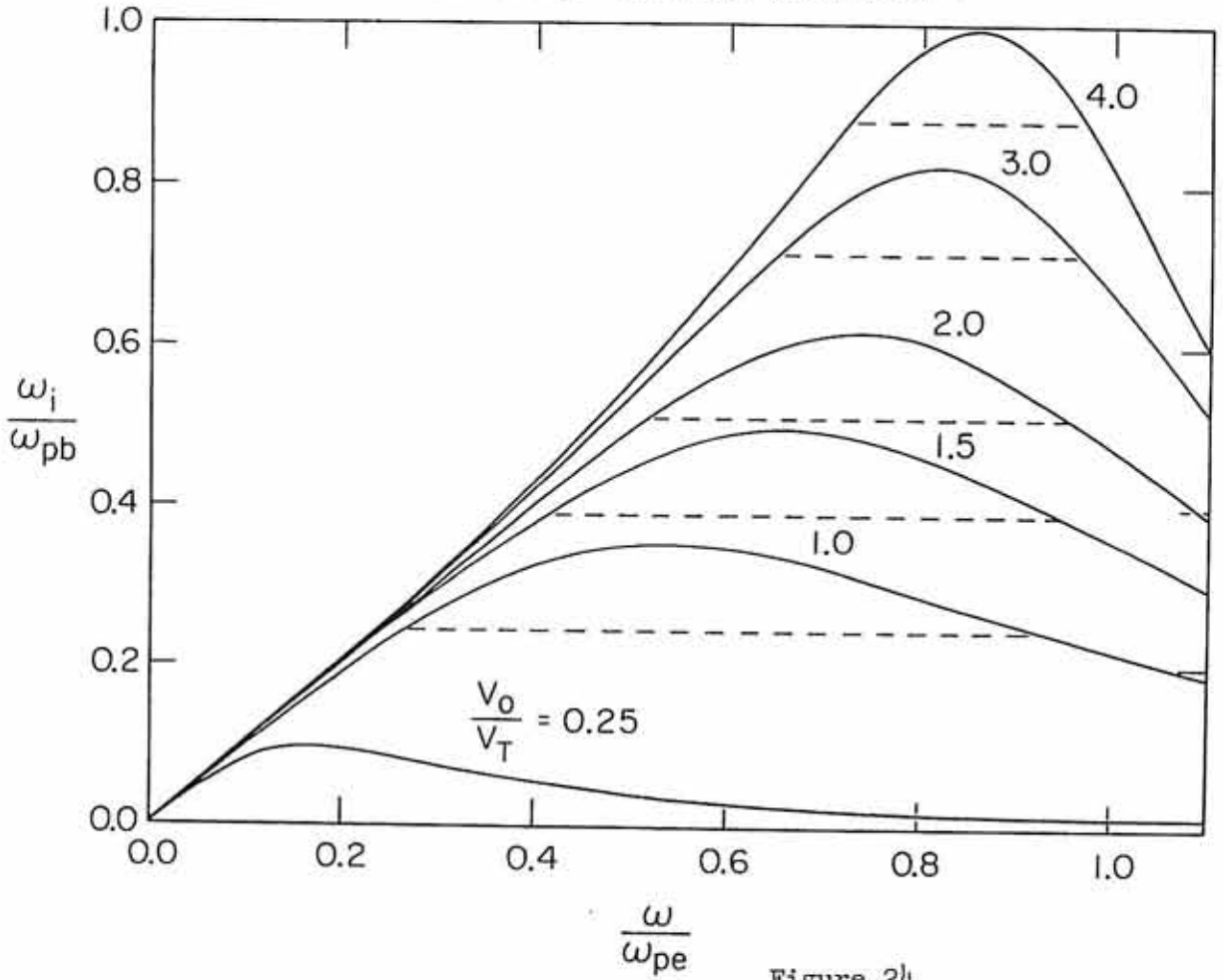

Figure 24

Figure 25 Graph of the frequency of the maximum growth rate of the resistive-medium instability versus V_o/V_T. This shows that for a range of V_o/V_T from about 1 to 5, the characteristic downshift in burst frequency below the plasma frequency is clearly explained.

A-G82-445

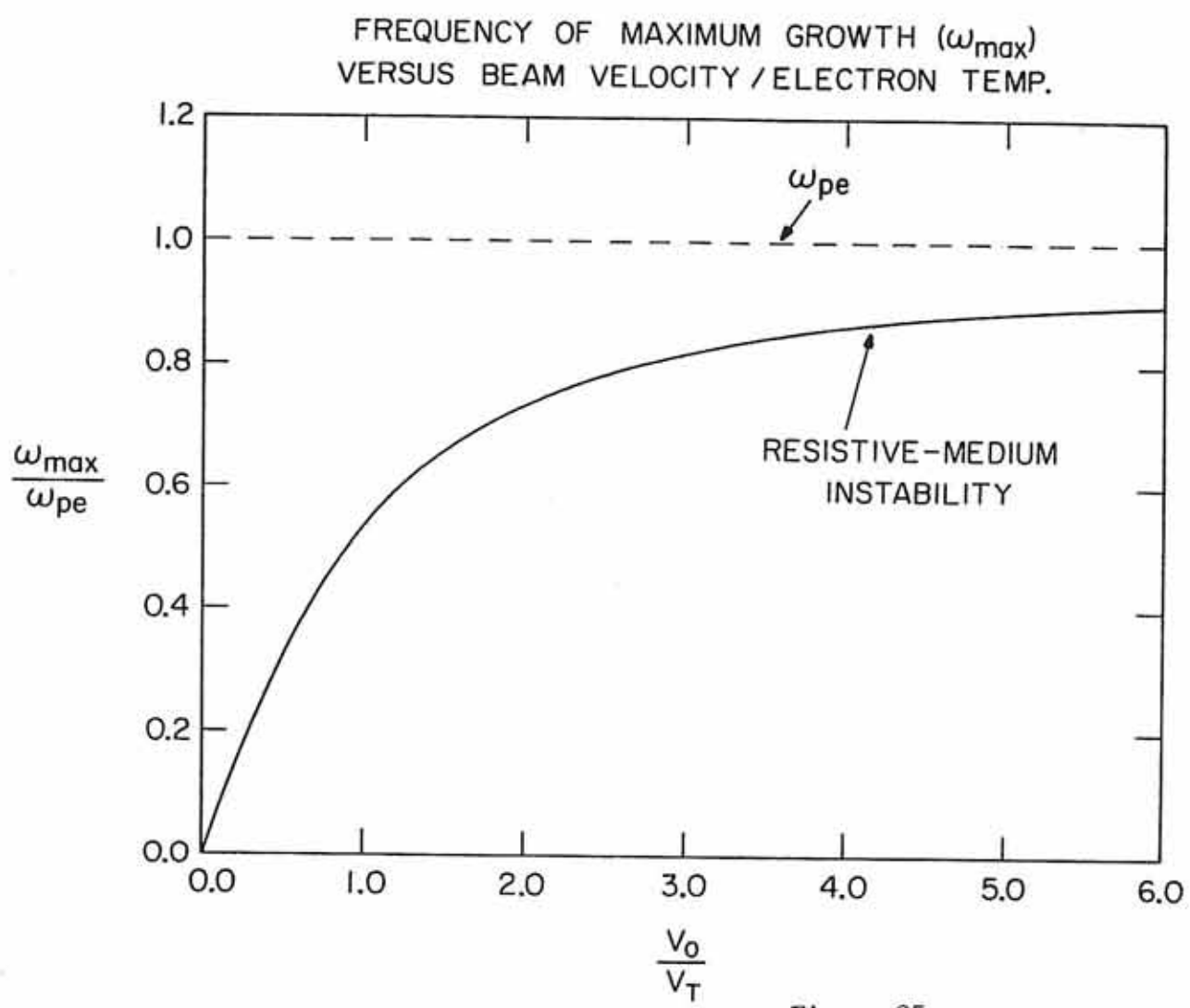

Figure 25

Figure 26 Plot of observed points in the wideband data showing the frequency bandwidth spread versus the downshift in the burst frequency below the plasma frequency. The theory points were made as described in the text using the graph shown in Figure 24.

A-G82-526

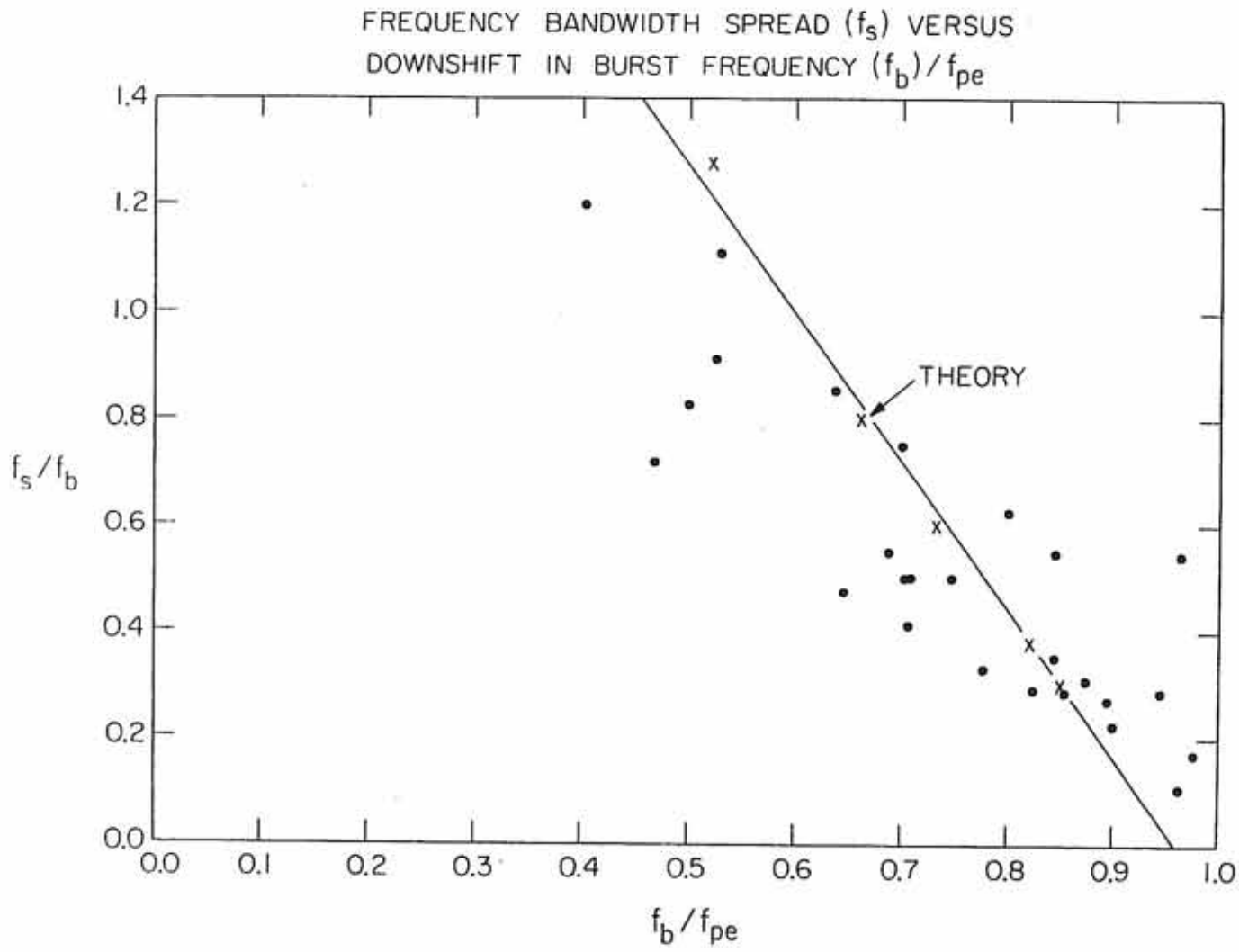

Figure 26

Figure 27 The lower panel shows some digitally transmitted wideband data from the Voyager 1 spacecraft when it was passing through the outer magnetosphere of Saturn in the dayside region. The bursts at about 8 kHz are suggestive of the type of chorus related electrostatic burst described in this study.

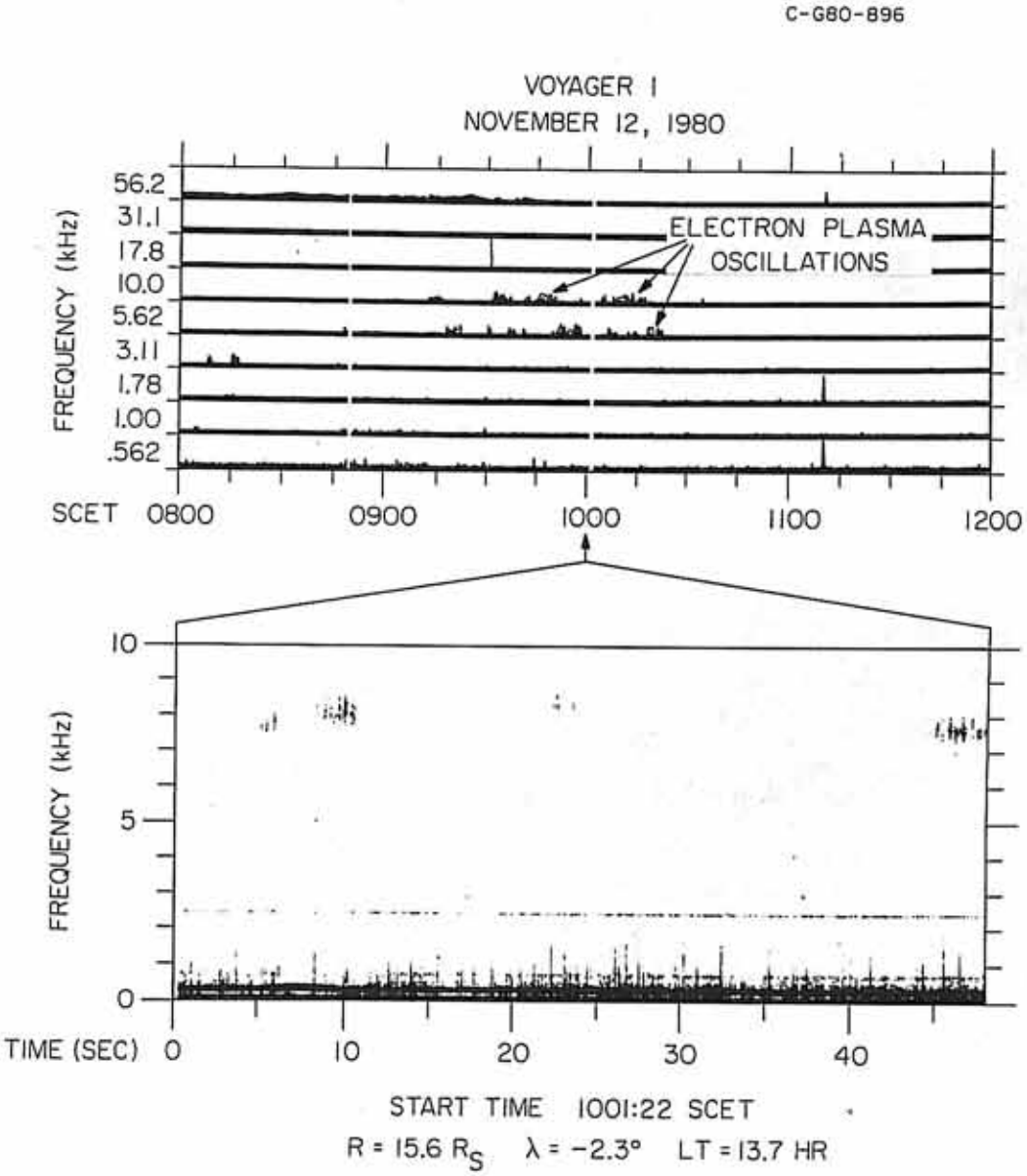
C-G80-896
VOYAGER 1
NOVEMBER 12, 1980
56.2
31.1
17.8
10.0
5.62
3.11
1.78
1.00
.562
FREQUENCY (kHz)
ELECTRON PLASMA
OSCILLATIONS
SCET 0800
0900
1000
1100
1200
10
5
0
FREQUENCY (kHz)
TIME (SEC) 0
10
20
30
40
START TIME 1001:22 SCET
R = 15.6 R_S λ = −2.3° LT = 13.7 HR

Figure 27

Figure 28 Diagram showing the energy flow and general cause-and-effect relationship for the model presented in this study.

A-G82-605

ENERGY FLOW

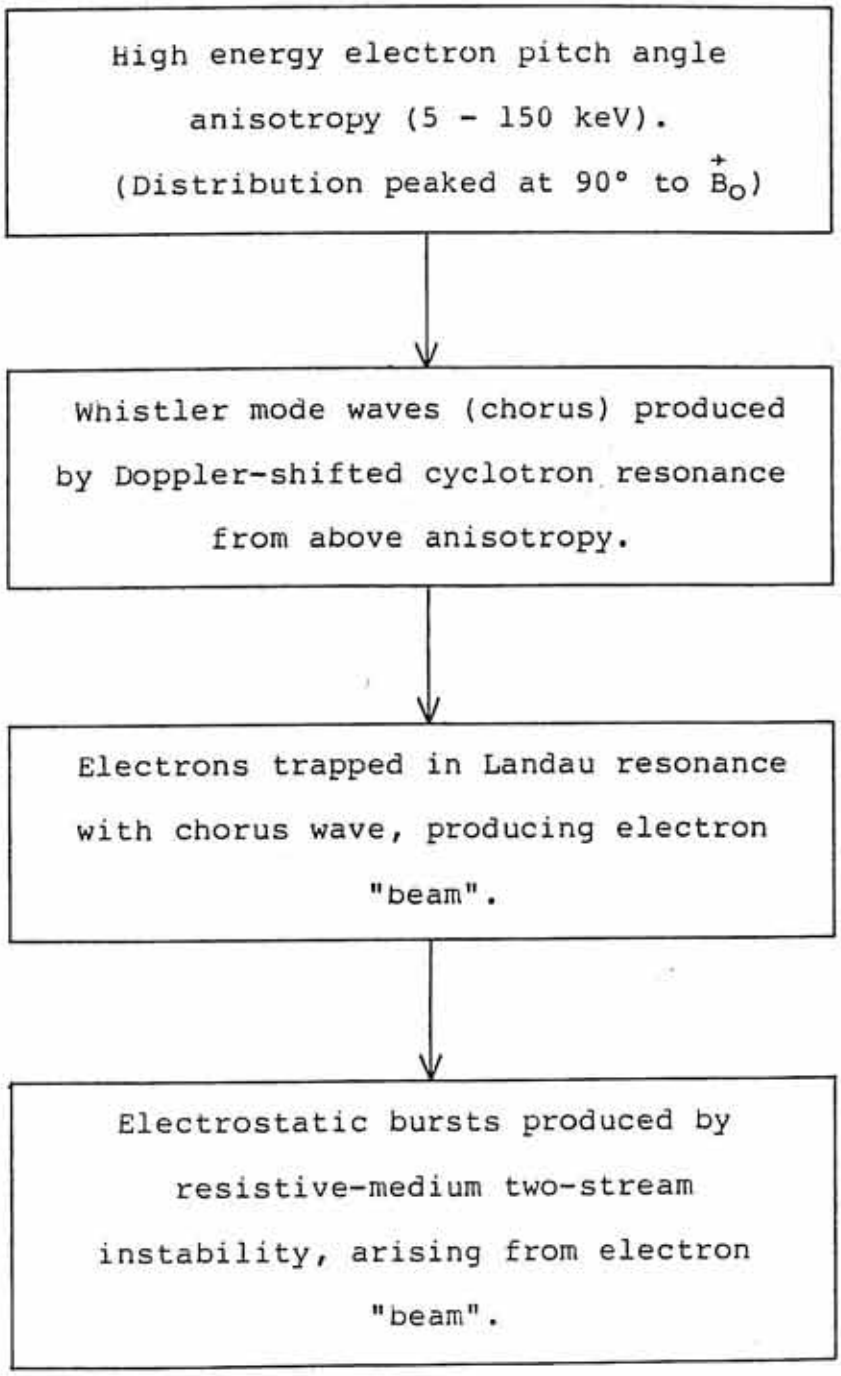

Figure 28